J. Math. Biol. (1995) 33: 619–660

Journal of Mathematical Biology

Selecting a common direction

I. How orientational order can arise from simple contact responses between interacting cells

Alex Mogilner, Leah Edelstein-Keshet

Department of Mathematics, University of British Columbia, Vancouver, BC V6T 1Z2, Canada
email: mogilner@math.ubc.ca, keshet@math.ubc.ca

Received 14 June 1994; received in revised form 10 November 1994

Abstract. We present results and analysis of models for contact-induced turning responses and alignment in populations of interacting individuals. Such models describe distributions of orientation, and how these evolve under different assumptions about the turning behaviour of individuals. One of these models was first used to describe interactions between mammalian cells called fibroblasts in Edelstein-Keshet and Ermentrout (1990) J. Math. Biol. 29: 33–58 (henceforth abbreviated EKE 1990). Here the original model is generalized to encompass motion in both 2 and 3 dimensions. Two modifications of this model are introduced: in one, the turning is described by a gradual direction shift (rather than abrupt transition). In another variant, the interactions between individuals changes as the density of the population increases to include the effects of crowding. Using linear stability analysis and synergetics analysis of interacting modes we describe the nature and stability properties of the steady state solutions. We investigate how nonhomogeneous pattern evolves close to the bifurcation point. We find that individuals tend to cluster together in one direction of alignment.

Key words: Cell alignment – Self-organization – Angular distributions

1. Introduction

In this paper we consider pattern formation phenomena in which patterns of angular (rather than spatial) distributions form. One can think of many biological examples in which alignment to a common direction or a set of common directions occurs: In a flock of flying birds or a school of fish, individuals moving together as a group orient to the same direction of motion (Grunbaum, 1994; Katz, et al., 1981; O'Brien, 1989). Alignment phenomena occur also in microscopic and in nonbiological systems: In liquid crystals,

rod-like molecules form various associations, including nematics, smectics, and cholesterics (de Gennes, 1974; Chandrasekhar et al., 1970; Greco and Marrucci, 1992; Luckhurst and Gray, 1979; Sheng, 1973). The type most closely related to the kind of order investigated in this paper are the nematic liquid crystals in which the molecules all have a common axis of alignment, but no long-range spatial order such as one commonly finds in the regular crystal structure. In a separate paper, (Mogilner and Edelstein-Keshet, 1994b) where both spatial and angular order are investigated, we find analogies with smectic-like order, where both long-ranged spatial order and alignment occur. We are interested in exploring how this spontaneous orientational order arises, what types of interactions promote this kind of pattern formation, and under what conditions.

This paper is a sequel to Edelstein-Keshet and Ermentrout (1990) which will be abbreviated EKE (1990). We further analyse a model for contact-alignment phenomena in a population of cells, **Model I**, first described there. However, we broaden the discussion to a more general exposition of the problem of orientational order and its mathematical analysis.

Aside from Model I, we consider also two related models. In **Model II** individuals gradually "drift" (rather than "jump") towards new directions of alignment. This is a more accurate description if interactions involve actual forces exerted by one unit on another. An example is actin-myosin interactions in the cytoskeleton of the cell. The third model (**Model III**), includes density-dependent turning rates. This could account for interactions in large populations in which the freedom of movement is restricted due to crowding.

Model I was first applied in EKE (1990) to populations of fibroblasts, mammalian cells that move by crawling. The cells are polar, having a "front" and a "rear". In the living body, cells navigate through a complex three-dimensional matrix. In artificial culture, the cells adhere to and move along the surfaces of their culture flask (on a 2D surface). The cells interact with one another as follows: If direct contact occurs between a cell and its neighbor, the contacting cell will either retract, or turn. This turning response forms the main phenomenon of interest here. **The response depends on the relative orientations of the participating cells.** The phenomenon at the population level is that cells initially randomly oriented can form patches of alignment called parallel arrays (Elsdale, 1972; Elsdale and Wasoff, 1976).

Model I consists of a pair of integro-partial differential equations which describe angular distributions of cells. The spatial distribution of the cells is not considered explicitly in this paper, but it is discussed in a companion paper by Mogilner and Edelstein-Keshet (1994c). Here we will make the assumption that the cells are distributed uniformly with respect to position.

Formation of preferred directions of alignment in a 2D region can be described as formation of pattern on a one-dimensional domain (the angular space θ) with periodic boundary conditions, $-\pi \equiv \pi$ or more simply, **pattern formation on a unit circle**. One goal in this paper is to generalize the analysis in EKE (1990) to angular distributions in 3D space, and this is analogous to a problem of **pattern formation on the unit sphere**. We also investigate the

influence of the drift term and the density-dependent term by comparing the first model with Models II and III. These models are suitable not only for cellular phenomena, but for some gross characterization of molecular phenomena. In a separate paper (Civelekoglu and Edelstein-Keshet, 1994) we describe structures formed by actin fibers crosslinked by actin-binding proteins. This problem also fits into the general scope of formation of orientational order. Some details about the associated phenomena in this case are given as examples in this paper. In a sequel to this paper (Mogilner et al., 1994b) we consider a limiting situation of a slow rotational diffusion leading to almost complete alignment. Here, in the first part, we concentrate on a parameter region close to the bifurcation value, so that the amplitude of the patterns are small.

The paper is organized as follows: Section 2 describes the models. Section 3 contains a summary of results of Model I based on EKE(1990). In Sects. 4, 5 and 6 we generalize these results to three dimensional rotations and introduce all necessary mathematical tools. The linear stability analysis is performed in Sect. 7. This is followed by nonlinear bifurcation analysis in Sects. 8 (2D) and 9 (3D). The Discussion lists a few related problems.

2. Description of the models

2a. Model I: Instantaneous alignment

As in EKE (1990), we restrict attention to cells distributed uniformly over space. We consider two groups of cells: those that are associated in groups ("**bound cells**") share a common axis of orientation and are restricted to motion along a single direction; those that are isolated ("**free cells**") can continually undergo random reorientation. Under the assumption that the medium is isotropic, and there is no preferred direction in the environment, it is reasonable to assume that the probability of alignment of two cells depends only on the relative angles between the cells. In Model I it is assumed that changes in orientation take place "instantaneously" when two cells align.

Definitions
t = time,
θ = angle of orientation relative to some arbitrary direction (e.g. the x axis),
$C(\theta, t)$ = density of free cells oriented with angle θ at time t,
$P(\theta, t)$ = density of bound cells oriented with angle θ at time t,
$K(\theta, \theta') = K(\theta - \theta')$ = probability of contact-induced turning from θ' to θ,
β = rate of alignment due to contact,
γ = rate of exchange between bound and free cells,
μ = rate of random turning by free cells.

In the original model it is understood that angles are taken in the range $-\pi \leqq \theta \leqq \pi$ and that functions of θ are periodic with period 2π.

Model I

As in EKE (1990) we consider the set of equations

$$\begin{cases} \dfrac{\partial P}{\partial t}(\theta, t) = \beta_1 CK * C + \beta_2 PK * C - \gamma P, \\ \dfrac{\partial C}{\partial t}(\theta, t) = \mu \dfrac{\partial^2 C}{\partial \theta^2} - \beta_1 CK * C - \beta_2 CK * P + \gamma P, \end{cases} \tag{2.1}$$

where we have used the usual notation for convolution,

$$K * C(\theta) \equiv \int_{-\pi}^{\pi} K(\theta - \theta')\, C(\theta', t)\, d\theta'. \tag{2.2}$$

In equations (2.1) μ represents the rate of random turning of free cells, and γ is the rate of shedding of cells from the bound fraction. The convolution term (2.2) captures the following elementary process of alignment: two free cells meet with initial directions θ, θ'. With some probability, say α, the cells continue moving with no interaction, and directions unchanged. With equal probability $(1 - \alpha)/2$ per unit time, the cells align to either direction θ or θ'. (The factor $(1 - \alpha)/2$ is absorbed into the constant β_1.) After aligning, the cells stick. (They become part of the class of bound cells.) The term $\beta_1 CK * C$ (which stands for $\beta_1 C(K * C)$) gives the rate at which free cells are converted to cells bound at angle θ through contact with other free cells. (The dimensions of this term are density increment per unit time).

If the interaction takes place between one free and one bound cell, it is always the free cell that re-orients. The term $\beta_2 PK * C$ is the rate at which free cells accumulate at angle θ due to contact with bound cells at that angle. By comparison, the term $-\beta_2 CK * P$ is the rate of loss of free cells from angle θ due to attraction to bound cells at any other angle (Note that these terms are NOT symmetric). The term $K * C$ can be viewed as a dimensionless expression which depends on the entire distribution $C(\cdot)$, but which acts at a given angle θ. We will refer to this expression **as the influence of the free cell distribution on the direction θ.** Similarly, we will refer to $K * P$ **as the influence of the bound cell distribution on the direction θ.**

As seen from the above equations, the approach is based on integro-differential equations. This imposes a non-local character to the model. Since there is little available information about the details of the alignment process, we do not consider in detail the time-rate of change of the cell direction. The latter approach is more appropriate when the nature of the forces causing rotation are known from basic physical principles, or from experimental evidence. Model II is appropriate for such cases.

2b Model II: objects subject to alignment force

In Model II we describe turning as a gradual rotation, rather than a spontaneous jump to a new orientation. This might be true if alignment was mediated

by some applied "force" (e.g. elastic tension). We describe the turning motion of the object as a rotation about its center of mass with some **angular velocity**. The angular velocity will stem from a force acting on the individual. In physics, many forces (such as those in electrostatics, but in particular any **conservative** force) can be expressed in terms of some underlying scalar potential function. It turns out that in Model II the kernels of the convolutions that describe interactions are most naturally interpreted as such potentials, as we illustrate below.

We define the angular velocity of an individual to be $\omega = d\theta/dt$. (Since we are here describing the model in 2D, $\omega = d\theta/dt$ is a scalar. Later the model will be generalized to 3D and then $\omega = d\boldsymbol{\Omega}/dt$ is a vector. Ω would then be the angle between two points Ω_1, Ω_2 on the sphere, and the direction of the vector $\boldsymbol{\Omega}$ is tangent to the arc joining Ω_1, Ω_2. We leave this generalization to a later section but here merely note that our definition of the angular velocity in 3D is different from the one common in mechanics.)

We will assume that the angular velocity is proportional to the corresponding force:

$$\omega \sim F_\theta \,, \tag{2.3}$$

The assumption of the proportionality of the velocity to the driving force comes from many biological applications. In the usual situation, in molecular and cell biology, very small objects move in highly viscous media, with relatively small speeds. Thus motion is characterized by low Reynolds numbers, for which **inertial forces can be neglected.**

We assume that the force F is conservative. Then F can be represented as a gradient of some corresponding **potential field** $\tilde{W}$:

$$F = -\nabla_\theta \tilde{W} \,. \tag{2.4}$$

In the simple 2D case,

$$\nabla_\theta \tilde{W} \equiv \frac{\partial}{\partial \theta} \tilde{W} \,.$$

In the 3D case,

$$\nabla_\theta \tilde{W} \equiv \partial \frac{\tilde{W}}{\partial \phi} + \frac{1}{\sin\theta} \frac{\partial \tilde{W}}{\partial \theta} \,.$$

The potential at a given angle θ is created by the sum total of interaction with individuals at all other angles. We assume linear superposition of forces. Then the potential $\tilde{W}$ can be written in the form:

$$\tilde{W} = W * C \equiv \int W(\theta - \theta')\, C(\theta', t)\, d\theta' \,. \tag{2.5}$$

Since each angle is associated with an angular velocity, objects tend to "drift" collectively. This drift can be described by a convection term in a canonical way. We assume simply that the flux associated with this drift is a product of the density and the velocity, i.e.:

$$J_0 = C\omega \tag{2.6}$$

Including the term $\varepsilon \Delta_\theta C$ for angular diffusion, leads to a balance equation for the angular distribution as follows:

$$\frac{\partial C}{\partial t} = \varepsilon_1 \Delta_\theta C - \nabla_\theta \cdot \boldsymbol{J}_\theta \,. \tag{2.7}$$

The drift term in equation (2.7) has the form

$$\nabla \cdot \boldsymbol{J}_\theta = \frac{\partial}{\partial \theta}(C(W' * C))$$

in 2D. This type of term appears in the models by [Grunbaum, 1994; Alt and Giegant, 1994] for chemotaxis and for actin-myosin interactions, respectively. In 3D this term would have the form

$$\nabla_\theta \cdot \boldsymbol{J}_\theta = \frac{1}{\sin\phi}\frac{\partial}{\partial \theta}(C(W' * C)) + \frac{1}{\sin\phi}\frac{\partial}{\partial \phi}(\sin\phi\, C(W' * C)).$$

Putting together equations (2.3–2.7) we arrive at

Model II

$$\frac{\partial C}{\partial t} = \varepsilon \Delta_\theta C - \nabla_\theta \cdot (C \nabla (W * C)) \,. \tag{2.8}$$

This equation describes the convectional drift of the objects in angular space towards the points of highest concentration, causing alignment. This tendency towards order competes with the dispersal influence of the diffusion.

2c Model III: Interactions at discrete angles

The third model can be viewed as a rough simplification of the second model, if we again drop the local nature of the interactions and introduce instantaneous jumps from an initial orientation to one resulting from an interaction. We use the same notation, C for density, and omit the distinction between free and bound objects, as in the second model. In this model, however, we cannot restrict ourselves to quadratic non-linearities, as in the case of the first two models. Careful check reveals that if the only nonlinearities are quadratic, and no distinction between different types of objects is present, then the following situation can occur: If there are two clusters of fully aligned objects of different sizes, then quadratic nonlinearities will not redistribute the objects, but diffusion will dissipate the peaks, so that pattern will not persist. This is not true of higher order nonlinearities. In a separate investigation (Mogilner and Ladizhansky, 1994) a version of cluster-interaction model which contains quadratic nonlinearities, but allows for a more general case of incomplete cluster alignment is described, revealing the possibility of angular order. (Incomplete alignment is mandatory, if the quadratic nonlinearities are to provide the drive for self-ordering.)

With the above considerations, we obtain the following equation:

Model III

$$\frac{\partial C}{\partial t} = C(Q(C) * C) + \varepsilon \Delta_\theta C \,. \tag{2.9}$$

Here the integral term is defined as:

$$Q(C) * C = \int_S d\theta' \, L(C(\theta) - C(\theta')) \, G(\theta - \theta') \, C(\theta', t) \,. \tag{2.10}$$

The kernel is now a product of two functions. The density dependent function $L(C(\theta) - C(\theta'))$ reflects the tendency for a bigger cluster to grow at the expense of the smaller cluster. The function G describes the angle dependence and has the same meaning and form as K in Model I. This is a rough approximation of the process of fast rotation of a small cluster of objects towards a more slowly moving big cluster, and their final merging. We assume that the function L is odd $L(-C) = -L(C)$, monotonous and bounded and $L'(0) > 0$. That L is odd means that the nonlinear term in equation (2.9) describes either growth or decay of the cluster at θ, depending on relative size of other clusters. Further, symmetry of the function L provides conservation of the total mass of the system.

2d Comments

Models I–III share several limitations:

A These models do not describe extremely low densities, for which we cannot successfully approximate stochastic processes of cell movement by continuous PDE's.

B The models are inappropriate for extremely high densities, either, as then topological packing constraints dominate all other effects (see Elsdale and Wasoff 1976; Onsager 1949).

C The binding rates of two free versus free and bound individuals are probably different, but we have neglected this distinction, taking $\beta_1 = \beta_2$ and using the same kernel to describe both events.

D One of the approximations we make is that we do not distinguish between cell clusters of different sizes. To have a detailed account of these, one would have to introduce the functions $P_2(\theta, t)$, P_3, P_4, . . . to denote clusters composed of two, three, four, . . . and n cells. The result would be a system of infinitely many equations for C, P_2, P_3, . . . which would lead to a complicated mathematical problem. Instead of doing so, we define the simplified variable $P = \sum_{n=2}^{\infty} nP_n$.

The detailed behaviour of the models depends in an interesting way on the nature of the kernels K, W, G. These kernels would have distinct properties in each model problem considered, as they are based on details of the biology

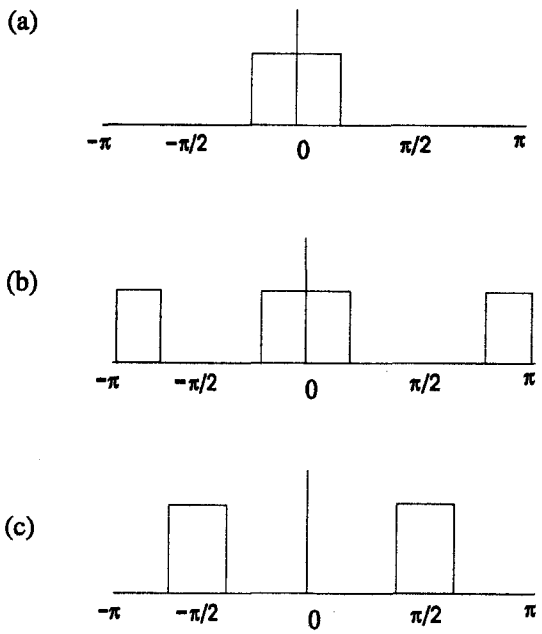

Fig. 1a–c. The kernels K used to represent the contact alignment phenomena are shown here as functions of the angle between cells. (In 2D the angle is θ, and in 3D it is γ.) **a** Single humped kernel, representing alignment in which both cells are oriented head-to-head. **b** Double humped kernel which permits cells to align also in a head-to-tail configuration. **c** An orthogonal interaction kernel that is not relevant for cellular interactions but that plays a role in the model for actin alignment. Some discussion of the properties of this kernel is given in Appendix IV. The figures illustrate kernels whose basic functional form is as for K_{II} in equation (A3.5)

that are either observed through experiments or conjectured from some knowledge of the system. In the case of fibroblasts, interactions causing alignment are known to be weakest if the cells meet at 90°. (see Fig. 1a,b). In the case of Actin fibers, crosslinking proteins of various sorts allow fibers to interact and bind at different configurations, including parallel and orthogonal structures (Civelekoglu and EK, 1994). The kernel is different in that case (see Fig. 1c). In parallel interactions, we must still consider a further distinction, namely whether alignment occurs only "head-to-head" or also "head-to-tail". The first case leads to a kernel with a **single hump** in the domain $-\pi < \theta < \pi$ (see Fig. 1a). The second case results in a kernel with a **double-hump** (see Fig. 1b). In this paper, we will focus attention mainly on the case of the single-humped kernel discussed in EKE (1990), i.e. on the case that cells align only head-to head, and not head-to tail. However, as we shall discuss, the case of the double humped kernel is a simple generalization of this situation which is obtained in 2D if angular space is changed from $[-\pi, \pi]$ to $[-\frac{\pi}{2}, \frac{\pi}{2}]$, and in 3D by an analogous change of angular space, Ω.

Both of the above types of kernels lead to parallel alignment of cells. In the case of Actin, where interactions can occur between orthogonal fibers, two

mutually orthogonal axes of orientation can be formed. The total mass of cells is equally distributed between these two axes. This case can be treated within the framework of a model essentially identical to Model I, provided the form of the kernel is suitably adjusted, as described later. (See, for example Fig. 1c or Civelekoglu and EK, 1994.)

In the original model, random turning is described by a second partial derivative, a diffusion-like term. The differential operator is the Laplacian operator in 1 (angular) variable, the continuum representation of a random walk. The equations are equivalent to a 1-space dimension PDE, but with the interpretation of the independent dimension as an angle, rather than a physical position. For this reason, the boundaries of the domain at $[-\pi, \pi]$ are periodic. When we ask whether the distributions of densities can become non-uniform, we are studying a problem of **pattern formation on a circle**. This observation is helpful when a generalization to 3D is made.

3. Summary of the behaviour of Model I

We first concentrate on the first model and briefly review results obtained in a previous publication (EKE 1990; Civelekoglu and EKE, 1994). (See also Appendix I.) We make several observations about the equations of Model I:

1. The total density of bound and free cells at all orientations, M, is a constant. This can be seen by integrating both sides of equations (2.1) and adding the two equations. Thus the equations admit a conserved quantity.
2. The equations have a homogeneous θ-independent steady state, $\bar{P}$, $\bar{C}$ in which
$$\bar{P}/\bar{C} = \beta M/\gamma \,. \tag{3.1}$$
3. The equations can be linearized about this steady state, yielding
$$\begin{cases} \dfrac{\partial P}{\partial t}(\theta, t) = \beta_1 \bar{C} K * C + \beta_2 \bar{P} K * C + \alpha C - (\gamma - \beta_2 \bar{C}) P \,, \\ \dfrac{\partial C}{\partial t}(\theta, t) = \mu \dfrac{\partial^2 C}{\partial \theta^2} - \beta_1 \bar{C} K * C - \beta_2 \bar{C} K * P - \alpha C + \gamma P \,. \end{cases} \tag{3.2}$$
for suitably defined constants α (see Appendix I).
4. These linearized equations contain two linear operators, (a) the Laplacian in 1D with periodic boundaries, and (b) the convolution on the same region. The set of eigenfunctions of the Laplacian in 1D, are simply the functions
$$\psi_n(\theta) = e^{in\theta} \quad n = 0, 1 \ldots . \tag{3.3}$$
or equivalently, sines and cosines of $(n\theta)$. The integer n is called the **mode number** (or the **harmonic number**). (It was also called the wavenumber, k in EKE (1990).) As discussed further in Appendix I, $(-n^2)$ is the eigenvalue corresponding to the eigenfunction $\psi_n = e^{in\theta}$.

5. A fundamental fact in this model is that the eigenfunctions of the Laplacian are also eigenfunctions of the linearized integral operator, with the property that
$$K * \psi_n = \hat{K}_n \psi_n, \quad n = 0, 1, \ldots \tag{3.4}$$
where $\hat{K}$ is the Fourier transform of the function $K(\theta)$, (see equation A1.4). We establish this important fact in Appendix I. We shall see below that the fact that the Laplacian and the integral operator share a set of eigenfunctions is essential in the analysis of the problem.
6. The linear analysis of this problem was explained in EKE (1990). Briefly, it was found that the homogeneous steady state could be destabilized by any perturbation of the form (A1.1) for modes n that satisfied the dispersion relation
$$An^2 < \hat{K}_n(1 - \hat{K}_n)\,, \tag{3.5}$$
where
$$A = \frac{\mu}{\gamma}\left(\frac{\gamma}{\beta M}\right)^2. \tag{3.6}$$
In the case of a single-humped kernel, it is found that the wavenumber $n = 1$ is the first destabilizing mode, whereas if the kernel has two humps, the first unstable mode is $n = 2$.
7. In Appendix I we show that the results for the double-humped kernel can be obtained from the single-humped case by suitably restricting the domain and defining the distributions $P_d(\theta)$, $C_d(\theta)$ in terms of the familiar solutions to the problem for the single-humped kernel case.
8. The case of the actin alignment kernel (Fig. 1c) is discussed in the Appendix IV. It is found that the wavenumber $n = 4$ is the first destabilizing mode, both in the 2D and the 3D cases. The mathematical treatment of this case is completely analogous to the single and double humped kernels, and therefore we omit detailed development.

4. Generalization of Model I to three-dimensional rotations

When rotational motion takes place in three dimensions, we must describe the set of possible directions by two angular variables, for example by the angles ϕ and θ used in spherical coordinates. A direction in 3D can be represented by a unit vector. Further, this vector can be identified with a point on the unit sphere. Thus if we were interested in the distribution of directions in a discrete population (composed of, say, M individuals), we could represent this by a distribution of M points on a unit sphere. However, as our models are concerned with continuous angular distributions in 3D, we shall deal with functions on the unit sphere. Thus, alignment of the cells is equivalent to formation of pattern on the unit sphere. (See, for example, Hunding, 1982.) We will interchangeably refer to "cells distributed at various orientations" and "cells distributed on the unit sphere". We shall use the angular coordinates $\Omega \equiv (\phi, \theta)$ to denote position on a unit sphere (see Fig. 2a). These coordinates

are defined with respect to a cartesian coordinate system by the usual spherical coordinate transformation

$$(x, y, z) = (\cos\theta \sin\phi,\ \sin\theta \sin\phi,\ \cos\phi)\ . \tag{4.1}$$

The previous problem can be generalized to 3D geometry by converting the operators to a fully 3D form. As in the 3D case, rotational diffusion can be represented as a random walk in the angular space, i.e., on the surface of a unit sphere. (See remarks in the Introduction.) Thus, this process can be described by the (angular part of the) Laplacian operator (Priestly et al., 1975). From here on, when discussing "the Laplacian" we shall refer only to the surface spherical part of the operator. We shall deal with the convolutions, which are simple generalizations in later remarks. We find that the equations can be written in the form

$$\begin{cases} \dfrac{\partial P}{\partial t}(\Omega, t) = \beta_1 CK * C + \beta_2 PK * C - \gamma P, \\ \dfrac{\partial C}{\partial t}(\Omega, t) = \mu \Delta C - \beta_1 CK * C - \beta_2 CK * P + \gamma P\ . \end{cases} \tag{4.2}$$

where now $P(\Omega, t)$ and $C(\Omega, t)$ are functions defined on a unit sphere. The Laplacian operator Δ in surface spherical coordinates is shown in Appendix II.

The convolutions are now done in 3D spherical geometry, so that

$$K * C \equiv \int K(\Omega, \Omega')\, C(\Omega')\, d\Omega'. \tag{4.3}$$

(See Appendix II for the full ϕ, θ form.) This expression can be interpreted as a clearcut analogue to the convolution in 2D. That is, we can think of $K * C$ as **the influence of the free cell distribution on the direction** $\Omega = (\phi, \theta)$. A similar interpretation can be made for $K * P$. It is necessary to generalize the definition of the kernel K to 3 dimensions in such a way that it is a function of the angle formed by the two directions (ϕ, θ) and (ϕ', θ') in space. We leave this detail to a later section.

For the sake of simplicity, we shall assume as in EKE (1990) that $\beta_1 = \beta_2$, i.e. that affinities of cells to other free or bound cells are identical. We feel that this assumption does not change the qualitative results of the model. The equations can then be brought into the following dimensionless form:

$$\begin{cases} \dfrac{\partial P}{\partial t}(\Omega, t) = CK * C + PK{*}C - aP, \\ \dfrac{\partial C}{\partial t}(\Omega, t) = \varepsilon \Delta C - CK * C - CK{*}P + aP\ . \end{cases} \tag{4.4}$$

where $a = \gamma/\beta, \varepsilon = \mu/\beta$. In this dimensionless formulation, we shall continue to refer to the convolutions as the **influence** of the cell distributions on the

particular direction Ω. We shall discuss the form and properties of the convolutions in a later section.

A similar generalization can be made in the case of each of Models II and III. The equations of these models are easily rewritten in terms of the spherical angle Ω.

5 Properties of the Laplacian in spherical coordinates

Linear stability analysis of the model (4.4) leads to a linear integro-partial differential equation problem, which together with the boundary conditions and geometry forms an eigenvalue problem. We consider separately the eigenfunctions and eigenvalues of the two operators that appear in the equations.

The Laplacian operator in this surface spherical geometry has as its eigenfunctions the **surface spherical harmonics** (SSH) $Y_n(\phi, \theta)$ of degree n with

$$\Delta Y_n = -n(n+1)\, Y_n \tag{5.1}$$

i.e. the corresponding eigenvalues are $\lambda_n = -n(n+1)$, $n = 0, 1, 2, \ldots$. The form of Y_n is given in Appendix II (equation A2.4) and involves a linear combinations of P_n^0, Legendre polynomials of degree n, and P_n^m, associated Legendre functions of degree n and order m (Macrobert, 1967; Kraut, 1979).

Due to symmetries of the sphere, the nth eigenvalue of the Laplacian has a $(2n+1)$-fold degeneracy. (There are $(2n+1)$ arbitrary constants in expression A2.4.) This fact plays a very important role in the bifurcation analysis of the 3D case. Note that due to this degeneracy of the spherical eigenfunctions, the eigenvalues depend only on n and not on m (see Macrobert, 1967). The first few Legendre polynomials for the case $m = 0$, namely, P_n^0, (usually written simply as P_n) are given in Appendix II.

6 Properties of the convolutions and their kernels in 3D

As in the 2D case, if we assume that the environment is isotropic, the interactions between two cells depend only on the relative angle of contact of these cells. In 2D this angle was simply $\theta - \theta'$, but in 3D it is a somewhat more complicated expression of the angles $\Omega \equiv (\phi, \theta)$ and $\Omega' \equiv (\phi', \theta')$. In 3D, the convolution $K * C$ takes the form

$$K * C \equiv \int_S K(\Omega - \Omega') C(\Omega')\, d\Omega', \tag{6.1}$$

where the integral is taken over the surface of the unit sphere S. We can write this convolution in terms of the angle between the two interacting individuals, γ, (see Fig. 2b) but it is more convenient to express it in terms of the cosine of this angle, $\cos\gamma$. Defining $\eta = \cos\gamma$, and rewriting the kernel as a function of

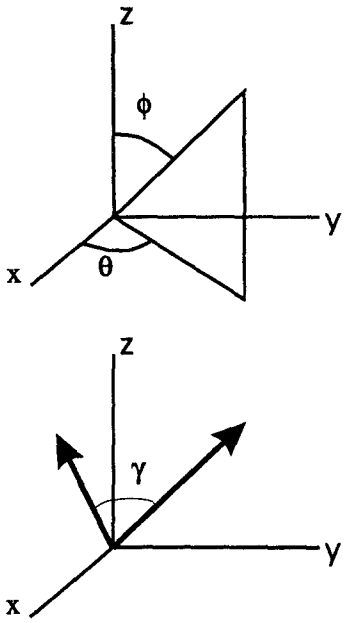

Fig. 2. **a** The angles ϕ and θ in spherical coordinates. **b** The angle γ between two directions in 3D

this argument (but with slight abuse of notation using the same symbol K for this new function), we have

$$K * C \equiv \int_0^{2\pi} \int_{-1}^{1} K(\eta)\, C(\phi', \theta') d(\cos\phi')\, d\theta' \,. \tag{6.2}$$

We observe that a vector dot product of the two vectors representing the interacting individuals produces a formula for $\cos\gamma$: Representing the directions of the cells by the two unit vectors

$$\begin{aligned} \boldsymbol{n} &= (\cos\theta \sin\phi, \sin\theta \sin\phi, \cos\phi)\,, \\ \boldsymbol{n}' &= (\cos\theta' \sin\phi', \sin\theta' \sin\phi', \cos\phi')\,. \end{aligned} \tag{6.3}$$

Forming the dot product, and rearranging algebraically leads to the result

$$\cos\gamma = \boldsymbol{n}\cdot\boldsymbol{n}' = \cos\phi\cos\phi' + \sin\phi\sin\phi'\cos(\theta - \theta')\,. \tag{6.4}$$

See Fig. 2b.

For stability analysis the crucial fact that we will later use is that the SSH are also eigenfunctions of the convolution operator K with the integral kernel $K(\Omega - \Omega')$. This result is analogous to the 2D case. (See discussion following equation (A1.3).) The appropriate eigenfunctions are now the set of functions $P_n^0(\eta)$, $n = 0, 1, \ldots$. This set is a complete orthonormal set of functions and we can thus write an expansion of the function $K(\eta)$ in terms

of these functions, i.e.:

$$K(\eta) = \sum_{n=0}^{\infty} K'_n P_n^0(\eta) , \tag{6.5}$$

where

$$K'_n = \frac{2n+1}{2} \int_{-1}^{1} K(\eta) P_n^0(\eta) d\eta . \tag{6.6}$$

in Appendix II (equations A2.6–2.8) we show that the inner products of the surface spherical harmonics (SSH) with the Legendre polynomials are also SSH. In 3D, we will use the notation

$$\hat{K}_n \equiv \hat{K}(n) = 2\pi \int_{-1}^{1} K(\eta) P_n^0(\eta) d\eta . \tag{6.7}$$

(This is convenient when interactions of modes are considered in a later section.) It is evident that $Y_n(\phi, \theta)$ are the eigenfunctions of the integral operator K and $\hat{K}_n$ are the corresponding eigenvalues. It is worth pointing out the similarity between these $\hat{K}_n$ for a given integer mode number n, in the 3D case and the Fourier transform $\hat{K}(n)$ for a given integer mode number n in the 2D case. Again we stress the similarity to the 2D case where eigenfunctions of both the Laplacian $\partial^2/\partial\theta^2$ and of the integral operator are the same.

We also comment that as in the 2D case, the expressions for transforms of the kernels $\hat{K}(n)$ are positive for $n = 1$ in the single hump case and for $n = 2$ in the double humped case, i.e. $0 \leqq \hat{K}_s(1), \hat{K}_d(2) \leqq 1$. (This follows from the fact that $\| P_n^0(x) \| \leqq 1$ which permits integral estimates of the transforms to be made, and from the normalization of the kernels.)

7. Linear stability results in 3D

Equations (4.4) have a homogenous steady state solution in which the distributions $\bar{C}$, $\bar{P}$ are constant for all directions in 3D. It is of interest to determine the stability of this steady state. In a way analogous to the 2D case, we consider a perturbation whose form is that of the eigenfunctions outlined in our discussion above, i.e.

$$\begin{bmatrix} P(\Omega, t) \\ C(\Omega, t) \end{bmatrix} = \begin{bmatrix} \bar{P} \\ \bar{C} \end{bmatrix} + \begin{bmatrix} P_0 \\ C_0 \end{bmatrix} Y_n(\Omega) e^{\lambda t}. \tag{7.1}$$

Details of the stability calculation are shown in Appendix III, and follow closely those in the 2D case. We find that in 3D, instability of the homogeneous distribution occurs at any harmonic n for which the following inequality is satisfied:

$$An(n+1) < \hat{K}_n(1 - \hat{K}_n), \qquad A = \frac{\mu}{\gamma}\left(\frac{\gamma}{\beta M}\right)^2 \tag{7.2}$$

Note that this equation is analogous to equation (3.5) for the 2D case. The coefficient A is identical, but the dependence on the degree of the harmonic n is slightly different.

Below we list conclusions which can be reached from the inequality (7.2):

1. To get some feeling for this inequality we chose several representative functional forms for the kernel $K(\gamma)$. In each of these cases, the kernel represents alignment only when objects meet at "small enough" contact angles (angle γ for which $\cos\gamma > 3/4$). Further, the kernels are all **single humped**, which means that anti-parallel interactions do not cause alignment. We have numerically plotted the functions on both sides of the inequality (7.2) for two values of the constant, $A = 0.1$ and $A = 0.03$ (see Figs. 3–5.) and for kernels of the form

$$K = \begin{cases} f(\gamma), & \cos\gamma > 3/4 \ ; \\ 0, & \cos\gamma < 3/4 \ , \end{cases} \tag{7.3}$$

with various functions f (see Appendix III equation A3.5) Each of these forms has finite support on a subinterval for which $|\gamma| < \pi/2$, but the kernels K_I, K_{II}, K_{III} have different types of discontinuities and shapes. It was shown in EKE (1990) that the exact functional form of $K(\theta)$ in 2D was not important, given its symmetry and type of support. Figs. 3(a,b,c) show the plot of the expression $\hat{K}_n(1 - \hat{K}_n)$ as a function of n for three kernels of the form (7.3) respectively. Figs. 4 and 5 show the parabolas on the right hand side of the inequality and the way that they intersect the curves of Fig. 3.
2. From these figures it is clear that as we decrease A symmetry breaks first as a result of the growth of the first harmonic. If A is much smaller, the second harmonic becomes unstable, then the third, fourth, etc in succession. However, it is not necessarily true that the mode $n = 1$ is the one that always breaks stability. In particular, if a kernel contains no components of the eigenfunction corresponding to this mode, one of the higher modes will cause instability.
3. A **double-humped** kernel occurs if interactions occur at angles both close to zero and close to 180°. The correspondence between the single-humped and the double-humped kernel K_d, is as follows:

$$\hat{K}_d(n) = \begin{cases} 0, & n \text{ odd} \\ \hat{K}_s(n), & n \text{ even} \ . \end{cases} \tag{7.4}$$

This holds provided the shape of K_d is identical to that of K_s but the periodicity is doubled. The result is that odd harmonics can never cause instability in the case of K_d, so that the break of symmetry is caused by the second harmonic.
4. Since A is positive, instability is most likely for low values of the integer n, for example for $n = 1$. Further, as we show in Appendix III, high harmonics cannot destroy stability.
5. In comparing the conditions for instability in 2D and 3D (i.e., the inequalities (3.7) and (6.10) we observe that in 2D the minimum value of the LHS of the instability criterion (3.5) when $n = 1$ is $\min_{n=1} An^2 = A$, whereas in 3D the minimum value of the LHS of (7.2) would be $\min_{n=1} An(n + 1) = 2A$.

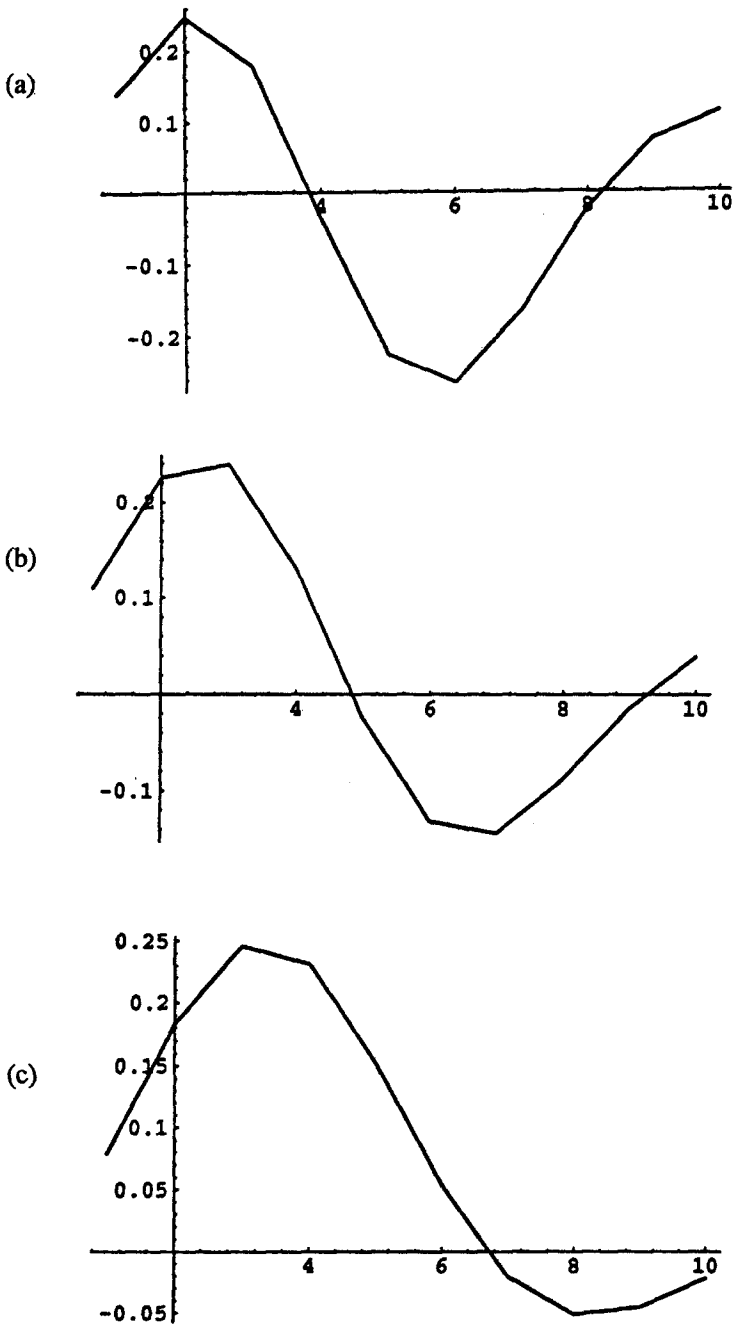

Fig. 3. **a** The expression $\hat{K}_n(1 - \hat{K}_n)$ which appears in the condition for instability given in the inequality (7.2) is shown plotted as a function of the mode n for the kernel K_I. Note that though the curves are shown as if they were continuous we are only interested in behaviour at integer values of n. The figure is generated using Mathematica to calculate the Legendre coefficients of the kernel. Note that only modes $n = 1, 2, 3$ can cause instability (this is the main region for which the graph is positive). **b** The same expression, but for the kernel K_{II}, **c** for K_{III}. In cases **b** and **c** the expression was calculated using the integral (6.7) for $\hat{K}_n$. **b** and **c** reveal a broader possible range of unstable mode numbers

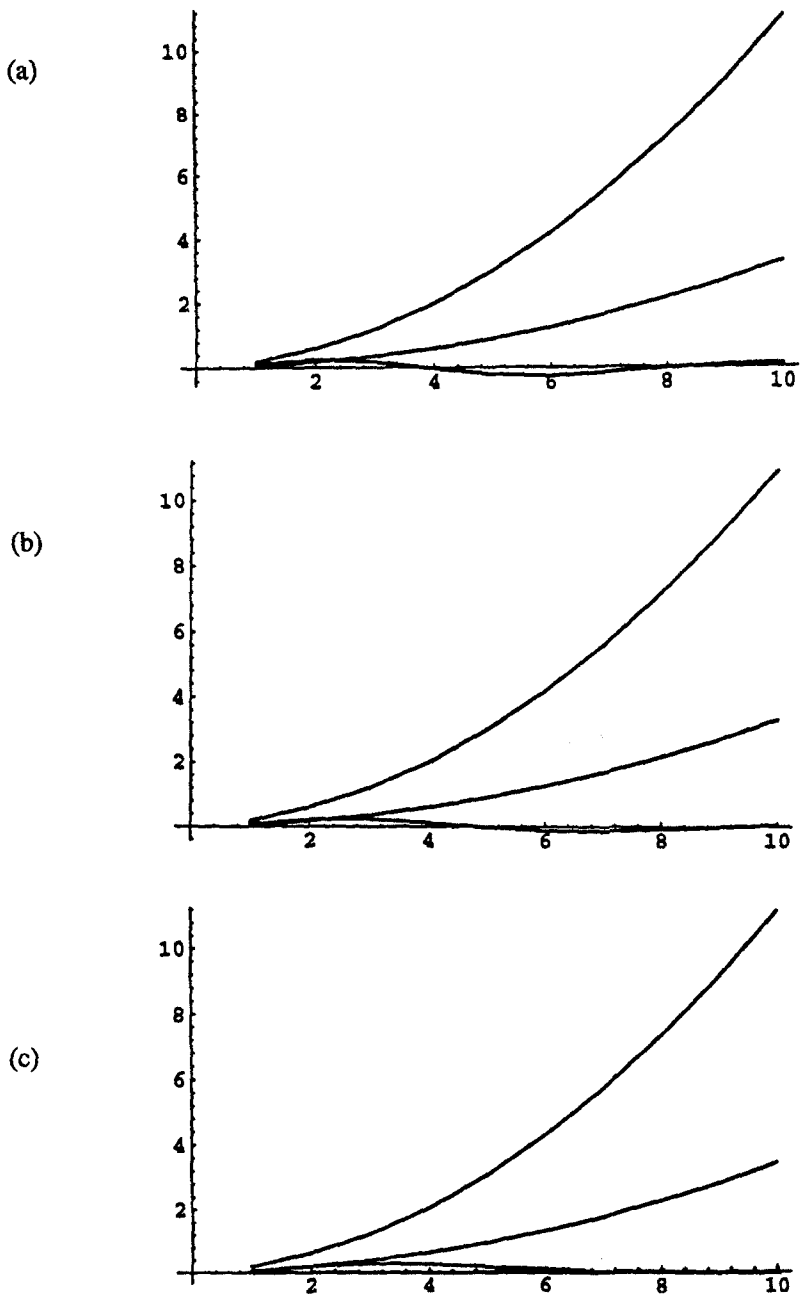

Fig. 4a–c. The same expressions as in Fig. 3 are plotted on a different scale. We also show the left hand side of the inequality, i.e. $An(n+1)$ as a function of n for $A = 0.1$ (top graph) and $A = 0.03$ (middle). Note that in this case the modes $n = 1$ and $n = 2$ will satisfy the (condition for instability

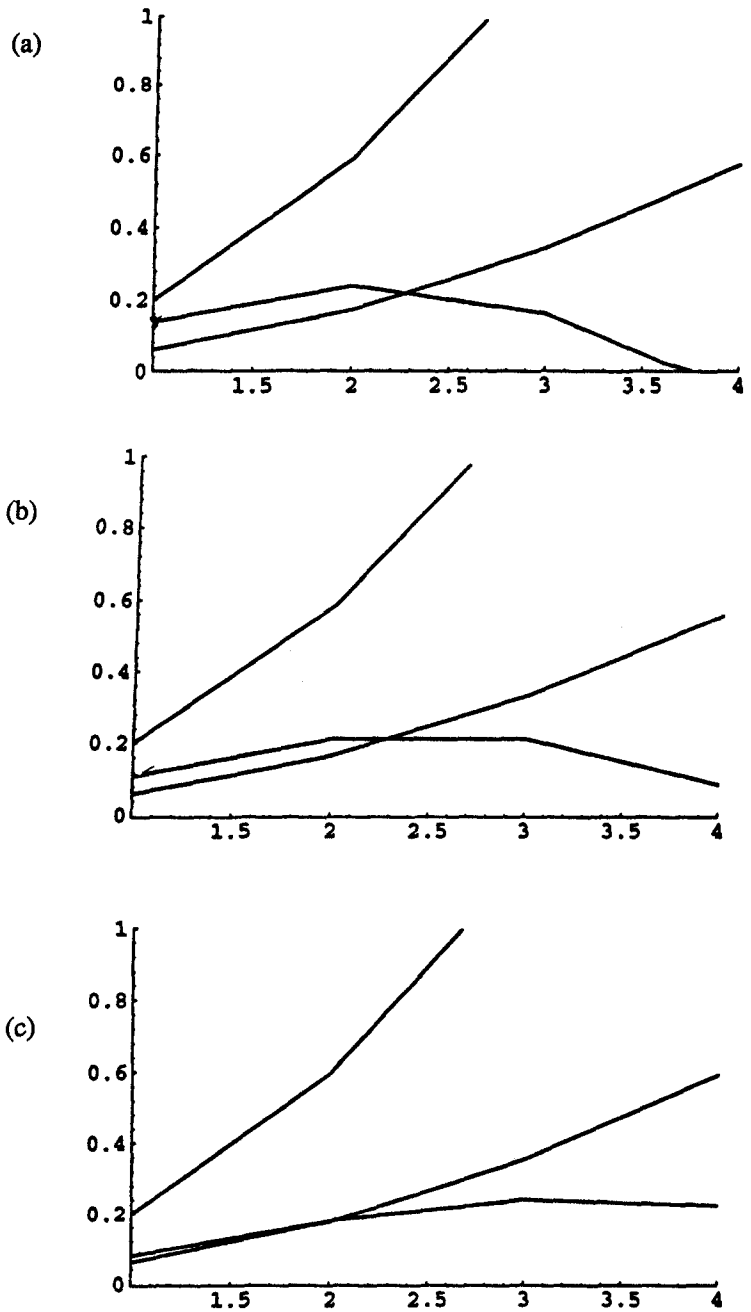

Fig. 5a–c. The same as in Figs. 3 and 4 but showing the region $0 < n < 4$ in more detail. The critical value of A, i.e. the one causing the onset of instability is $A_{cr} \approx 0.08$ in **a**, $A_{cr} \approx 0.06$ in **b**, and $A_{cr} \approx 0.04$ in **c**

The right hand sides of both inequalities are the same, and in both cases the expression attains a maximum value of $\max(\hat{K}_n(1-\hat{K}_n)) = \frac{1}{4}$. Thus, if $A > 1/4$ in 2D or $A > 1/8$ in 3D, the homogeneous state is stable. This shows that the homogeneous state tends to be more stable in 3D. This makes physical sense also because of the larger number of diffusional degrees of freedom in 3D that can destroy order.

6. We can construct a particular form of the kernel, which would be most likely to guarantee existence of a non-homogeneous solution by using the above properties. See Appendix III for details.
7. We can think of two possible extreme cases. If the function K is a constant, then the function $\hat{K}$ is δ-like. This corresponds to the situation in which cells can interact equally with all cells at every other angle. Conversely if K is a δ-like function then $\hat{K}$ is a constant. This corresponds to the case that cells interact only with other cells at nearly the same orientation. In either one of these extremes, if we perform all calculations as above, it is found that the homogeneous state is stable. (Details are omitted.)

Let us now consider the stability for Models II and III. Both these models contain a single equation, so the analysis is quite simple. In both models the homogeneous solution in which the distribution $\bar{C}$ is constant for all directions is stationary. We substitute the pattern

$$C(\Omega, t) = \bar{C} + C_0 z_n(\Omega)\, e^{\lambda t} \tag{7.5}$$

into the equations (2.8, 2.9) and keep terms linear in C_0. Then instability to growth of the nth mode would occur whenever $\lambda > 0$.

Model II

The instability criterion has the form (both in 2 and 3D):

$$\varepsilon < \bar{C}\hat{W}_n \tag{7.6}$$

This can be seen readily from equation (2.7): In Fig. 6 this inequality is illustrated graphically for the following step kernels: In 2D:

$$W(\theta) = \begin{cases} \frac{1}{2a}, & -a < \theta < a \\ 0 & \text{otherwise} \end{cases} \tag{7.7a}$$

and in 3D:

$$W(\Omega) = \begin{cases} A_2, & \cos\gamma > \frac{3}{4} \\ 0, & \cos\gamma < \frac{3}{4} \end{cases} \tag{7.7b}$$

Model III

Using the fact that at small C we have $L(C) = \eta C + O(C^2)$, we obtain the following instability criterion:

$$\eta\bar{C}^2(1-\hat{G}_n) > \varepsilon \begin{cases} n^2, & \text{in 2D} \\ n(n+1), & \text{in 3D} \end{cases} \tag{7.8}$$

The inequality is illustrated in Fig. 7 for the same kernels as the ones used for Model II.

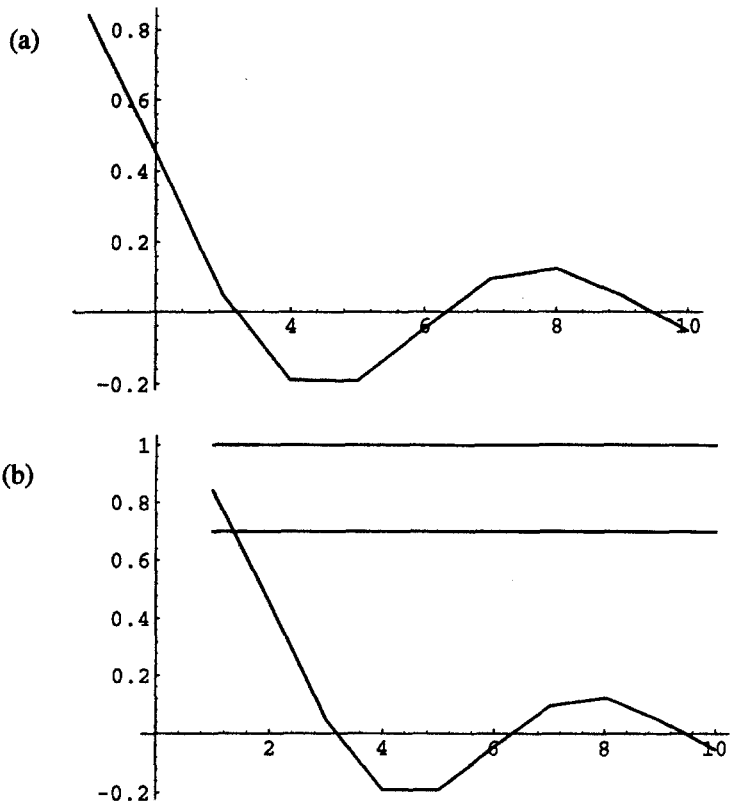

Fig. 6. **a** The expression $\bar{C}\hat{W}_n$ which appears in the condition for instability for Model II given in the inequality (7.6) is shown plotted as a function of the mode n for the kernel (7.7a) in 2D. **b** The same expression as in **a**, but shown together with superimposed lines representing two possible values of ε (left hand side of the inequality 7.6), namely $\varepsilon = 1.0, 0.7$. It can be seen that the inequality (7.6) is satisfied in the latter case and instability to the mode $n = 1$ occurs. **c** As in **a** but for the kernel (7.7b) in 3D. **d** Same as **b** but in 3D. The values $\varepsilon = 0.3, 0.2$ are shown. Instability to $n = 1$ occurs for $\varepsilon = 0.2$

The statements 1–4 for the case of Model I hold also for Models II and III. In particular, as ε is decreasing, stability is broken first by the first harmonic ($n = 1$) for single humped kernel and by the second harmonic for the double humped one.

8. Bifurcation analysis of Model I in 2D

In order to understand the pattern that arises after stability of the homogeneous distribution is lost, we apply an analysis based on the **synergetics** approach, as outlined by Haken (1977), Friedrich and Haken (1989). The basic idea of this approach is that close to bifurcation, the fastest growing mode essentially controls the amplitudes of other modes which are just becoming unstable. This is the so-called adiabatic or "slaving" principle of synergetics.

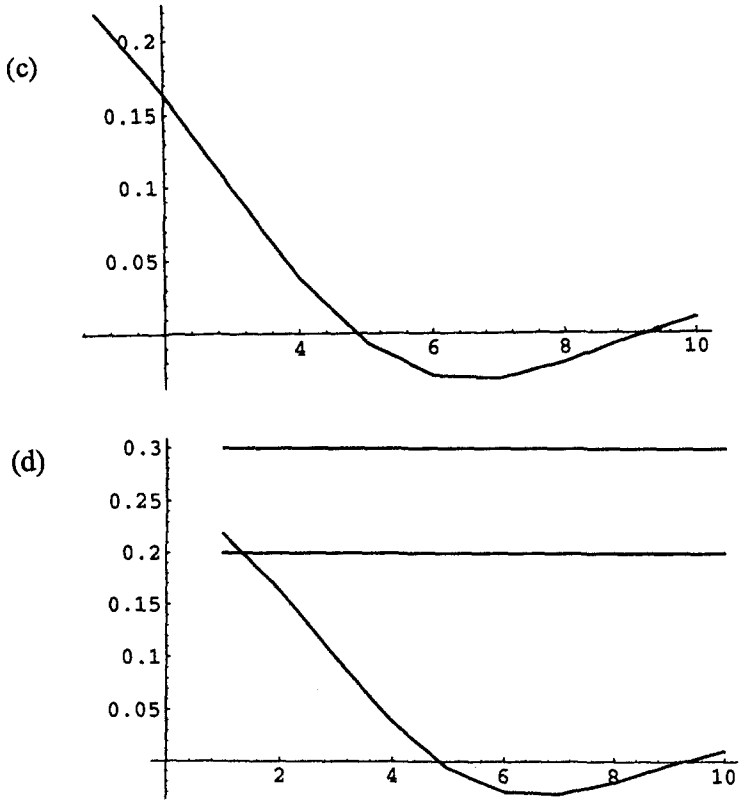

Fig. 6 (continued)

The reason that this assumption can be made is as follows: When the amplitudes of all harmonics are very small, the unstable mode grows exponentially. Further, the relaxation time of the stable modes is small relative to the time scale of variation of the unstable mode. This means that the stable modes will quickly reach meta-stable states and thereafter slowly follow the dynamics of the unstable mode. These facts lead to an increase in the amplitude of the first mode at the expense of the other modes.

We begin with the 2D case having $O(2)$ rotational symmetry. (We shall see that results are dependent on this symmetry.) We will assume that the first harmonic is responsible for the stability break, that is, that the growth rates of other modes are all negative, ($\lambda_n < 0, n = 2, 3, \ldots,$) and the first mode is just beginning to grow ($\lambda_1 > 0, \lambda_1 \approx 0$). Then this unstable harmonic will be the leading mode, but its magnitude is small compared to the magnitudes of the decay rates of the other modes close to the onset of instability ($|\lambda_1| \ll |\lambda_i|, i = 2, 3, \ldots$).

Details of the calculations, which rely heavily on the above assumptions are given in Appendix V. As a first step we express the state in terms of

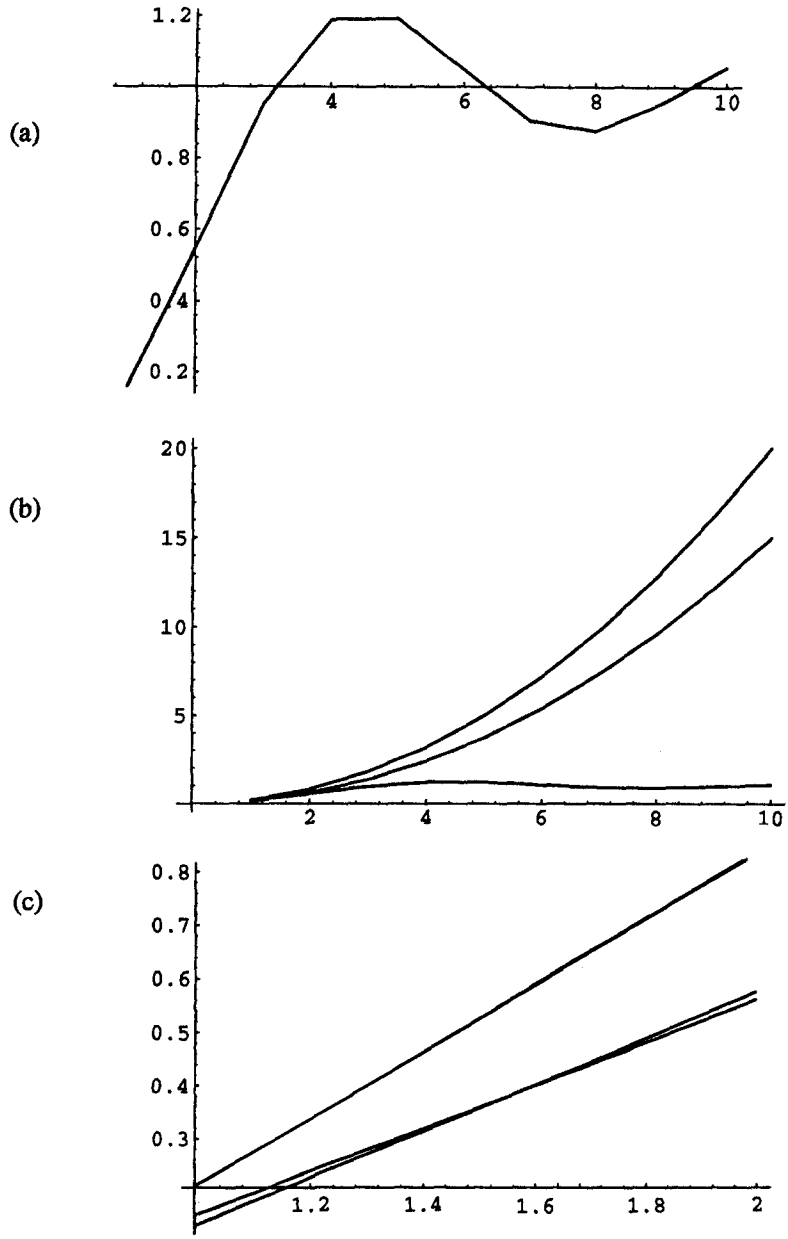

Fig. 7. **a** The expression $\eta \bar{C}^2(1 - \hat{G}_n)$ which appears in the instability condition (inequality 7.8) for Model III is shown plotted as a function of the mode n for the kernel (7.7a) in 2D. **b** The same expression as in **a**, with a superimposed graph of the expression εn^2 (right hand side of inequality (7.8) for two possible values of ε, namely $\varepsilon = 0.2, 0.15$. The smaller ε value causes instability to $n = 1$. **c** The same as **b**, but showing the region $0 < n < 2$ in greater detail. **d** As in **a**, but for the kernel (7.7b) in 3D. **e** The expression in **d**. We also show the expression $\varepsilon n(n + 1)$, the right hand side of inequality (7.8) for two possible values of ε, namely $\varepsilon = 0.2, 0.4$. **f** The same as **e** but showing the region $0 < n < 3$ in greater detail

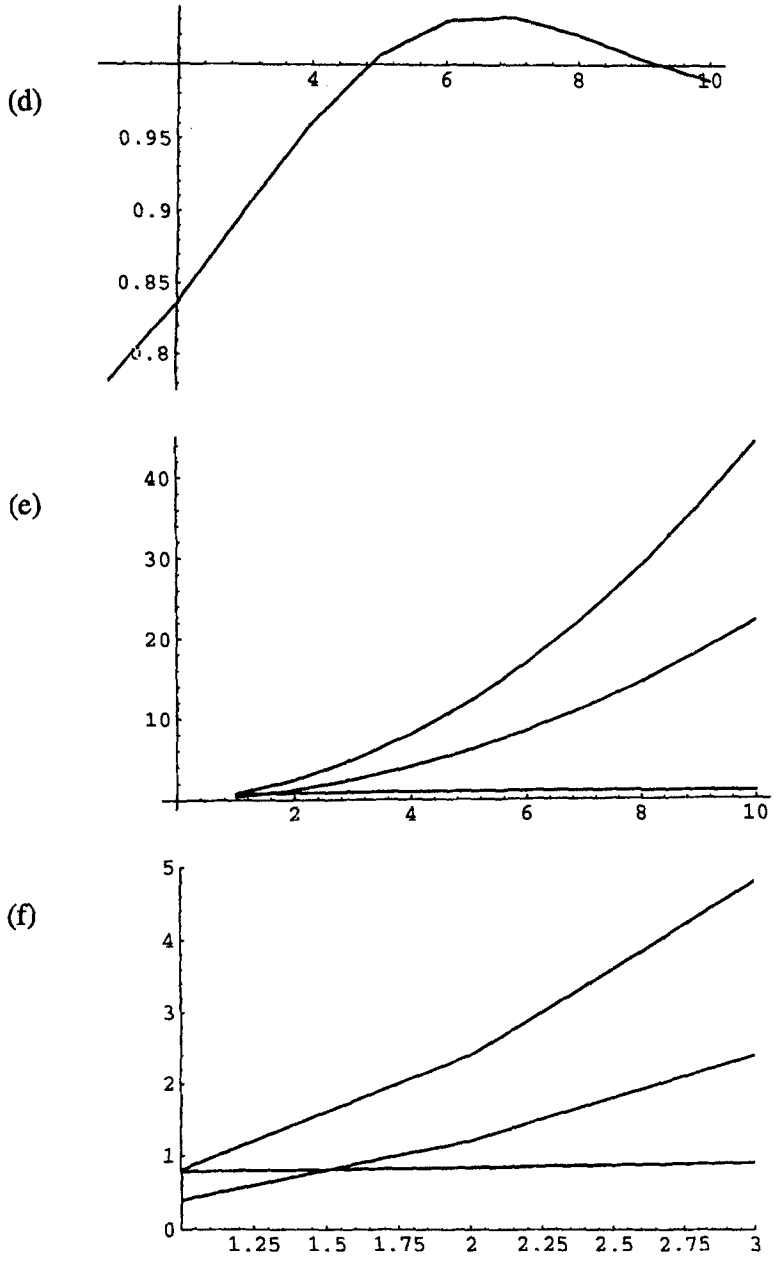

Fig. 7 (continued)

a superposition of the steady state, the growing first harmonic, and the other harmonics.

$$\left(\frac{C(\theta,t)}{P(\theta,t)}\right)=\left(\frac{\xi_1(t)}{\eta_1(t)}\right)v_1(\theta)+\sum_{i=2}^{\infty}\left(\frac{\xi_i(t)}{\eta_i(t)}\right)v_i(\theta)+\left(\frac{\bar{C}}{\bar{P}}\right). \tag{8.1}$$

In this expansion, the values $(\xi_i(t), \eta_i(t))$ are time-dependent amplitudes of the given harmonics, and these are assumed to depend on the amplitude of the first mode. This assumption is valid close to criticality where the behaviour of the system is entirely determined by the single unstable mode. The amplitudes of all the other modes are small, so it is possible to form a valid asymptotic expansion for $\xi_i(t)$ and $\eta_i(t)$ in powers of the unstable mode amplitudes ξ_1, and η_1, as shown in equation A5.3 of Appendix 5.

This approach allows us to eliminate the amplitudes of the stable modes and leads to a closed set of ordinary differential equations for the unstable amplitudes, the so called **generalized Ginsburg-Landau equations**:

$$\frac{\partial}{\partial t}\begin{pmatrix}\xi_1\\ \eta_1\end{pmatrix} = \lambda_1\begin{pmatrix}\xi_1\\ \eta_1\end{pmatrix} + \boldsymbol{P}\{\xi_1, \eta_1, \xi_i(\xi_1, \eta_1), \eta_i(\xi_1, \eta_1)\}, \quad i = 2, \ldots \tag{8.2}$$

where $\boldsymbol{P}$ is a non-linear functional.

If we were to analyze the steady state solutions of this set of ordinary differential equations we would get a detailed description of pattern created close to bifurcation. We will here explore a simplified version of this approach, looking only for the time-independent solutions, and not for the full time behaviour for which the calculations are forbidding. That is we set

$$\frac{\partial P}{\partial t} = \frac{\partial C}{\partial t} = 0\,. \tag{8.3}$$

This leads to the following pair of equations:

$$\begin{aligned} C(K * C) + P(K * C) - aP &= 0\,,\\ \varepsilon \Delta C - C(K * C) - C(K * P) + aP &= 0\,, \end{aligned} \tag{8.4}$$

(where now, in the 2D case, $\Delta \equiv \partial^2/\partial\theta^2$). From equations 8.4 we deduce that

$$P = \frac{C(K * C)}{a - (K * C)}\,. \tag{8.5}$$

Inserting (8.5) into (8.4b) we obtain

$$\varepsilon \Delta C + V(C) \cdot C = 0\,, \tag{8.6}$$

where

$$V(C) = \frac{(K * C)^2}{a - (K * C)} - K * \left(\frac{C(K * C)}{a - (K * C)}\right). \tag{8.7}$$

We now look for a solution of equations (8.6–8.7) in which the deviation away from the homogenous state is expressed as a superposition of the harmonics, as discussed above, in equation (8.1). That is we let

$$C(\theta) = \bar{C} + \xi(\theta), \quad |\xi(\theta)| \ll \bar{C} \tag{8.8}$$

where $\xi(\theta)$ is explicitly expressed as a mode superposition (See Appendix equation A5.4). The strong inequality in (8.8) holds close to criticality.

Suppose we were to restrict attention to the linear approximation, i.e. retain only terms that were linear in ξ. (We show that this is **not** informative as follows:) The linear approximation is

$$\varepsilon \frac{\partial^2 \xi}{\partial \theta^2} + a\left(\frac{\bar{C}^2}{(a-\bar{C})^2}\right)[(K*\xi) - K*(K*\xi)] = 0 \tag{8.9}$$

Substituting in the full mode expansion for $\xi(\theta)$ into this equation and equating coefficients of each harmonic on both sides of the resulting equation, leads to a set of equations, one for each mode amplitude ξ_n. These equations are of the form:

$$\lambda_n \xi_n = 0, \quad n = 1, 2, \ldots \tag{8.10}$$

where the coefficient λ_n coincides with an eigenvalue of the stability matrix, as shown in Appendix V).

These equations have only trivial solutions, which indicates that the linear approximation is not sufficiently informative. Thus, it is apparent that the nonlinear terms, which will lead to the interactions between harmonics are essential. According to the synergetics approach, the terms of up to third order of smallness are needed in the expansion. That means that terms of the form $(K*\xi)^2, (K*\xi)(K*(K*\xi)), K*((K*\xi)^3), \xi^2(K*\xi)$ and so forth must be retained in the equation for ξ. As this equation is rather cumbersome, we leave its details to Appendix V (equation A5.7).

The next step, as before, is to substitute the mode expansion of $\xi(\theta)$ into the nonlinear equation and keep terms up to third power in the leading mode, ξ_1 and up to second power in all other modes ξ_i, $i = 1, 2, \ldots$. We justify this since by the "Slaving Principle" the magnitudes of all modes are much smaller than that of the leading mode. After some simplification we equate coefficients of each harmonic on both sides of the equation as before. This calculation leads to a system of equations (one equation for each mode). The system has a particular hierarchical structure which makes it straightforward to solve:

$$\begin{cases} \lambda_1 \xi_1 + B_1 \xi_1 \xi_2 + F\xi_1^3 + G\xi_0 \xi_1 = 0 \ , \\ |\lambda_2| \xi_2 + B_2 \xi_1 \xi_1 + B_2^1 \xi_1 \xi_3 = 0 \ , \\ |\lambda_3| \xi_3 + B_3 \xi_1 \xi_2 + B_3^1 \xi_1 \xi_4 = 0 \ , \\ \vdots \\ |\lambda_n| \xi_n + B_n \xi_1 \xi_{n-1} + B_n^1 \xi_1 \xi_{n+1} = 0 \ . \end{cases} \tag{8.11}$$

Note that the first equation involves only ξ_0, ξ_1, ξ_2, the second equation only ξ_1, ξ_2, ξ_3, etc., so that they can be solved one at a time. The coefficients B_i, B_i^1, F, G are given explicitly in equation (A5.8) of the appendix, and are of order 1. Further, using the fact that the total mass, $M = C + P$ is constant leads to the estimate

$$\xi_0 \simeq -A_1 \xi_1^2 \ , \tag{8.12}$$

where A_1 is given in equation (A5.8). The fact that the amplitude of the leading mode dominates strongly over all other modes means that the terms whose

coefficients are B_n^1 in equation (8.11) above can be neglected compared to the other terms in each equation, further simplifying the task of solving the set of equations. We thus estimate the amplitudes of the stable modes as follows:

$$\xi_n \simeq \frac{B_n}{\lambda_n} \xi_1 \xi_{n-1} \,. \tag{8.13}$$

We observe that this implies that the modes are strictly ranked in size, i.e. that $|\xi_n| \ll |\xi_{n-1}|$. Plugging (8.12) and (8.13) for $n = 2$ into the first equation of the system (8.11) we obtain a self-contained equation for ξ_1 whose form is:

$$\lambda_1 \xi_1 - D\xi_1^3 = 0 \,, \tag{8.14}$$

(see Appendix for details). Careful estimates reveal that the coefficient D in this equation is positive unless the total mass M is very small ($M \ll a$; but then $\bar{C}$ is very small and of the same order of magnitude as ξ, so that the above method then cannot be applied). Thus, the solution of (8.14) has the form:

$$\xi_1 = \pm \sqrt{\frac{\lambda_1}{D}} \,. \tag{8.15}$$

We now consider a and M as constants and introduce the idea of a governing parameter, ε, (which may be some combination of original parameters of the model). We assume that as this parameter crosses a critical value, ε_c, stability breaks. Very close to this critical value, i.e. when $(\varepsilon - \varepsilon_c) \ll \varepsilon_c$ we can write (8.15) in the more revealing form

$$\xi_1 = \pm k \sqrt{|\varepsilon - \varepsilon_c|} \,. \tag{8.16}$$

Further, using the estimate (8.13) gives us the additional result

$$|\xi_n| = k_n |\varepsilon - \varepsilon_c|^{n/2}, \quad n = 2, \ldots \tag{8.17}$$

where k, k_n are some coefficients of finite order. We have thus explicitly recast the amplitudes of all modes in terms of the governing parameter, ε, and more specifically, in terms of its "distance" from the critical value at which bifurcation occurs.

The bifurcation diagram based on these results appears in Fig. 8. It can be seen that the bifurcation is supercritical, implying a non-equilibrium phase transition of second order. [See Friedrich and Haken, 1989.] This means that as the parameter ε increases past the critical value, the amplitude of the nonhomogeneity increases gradually from zero. This resembles the dynamics of growth of the **order parameter** in physical systems such as liquid crystals.

So far we have assumed a single humped kernel. In the case of a double humped kernel, we have an expansion over the even harmonics only; the second harmonic is then responsible for the stability break in general. In this case the reasoning and the mathematical derivations are entirely analogous to the case we have discussed in detail. The expansion is shown in detail in Appendix V (equation A5.10) and the character of the bifurcations is the same.

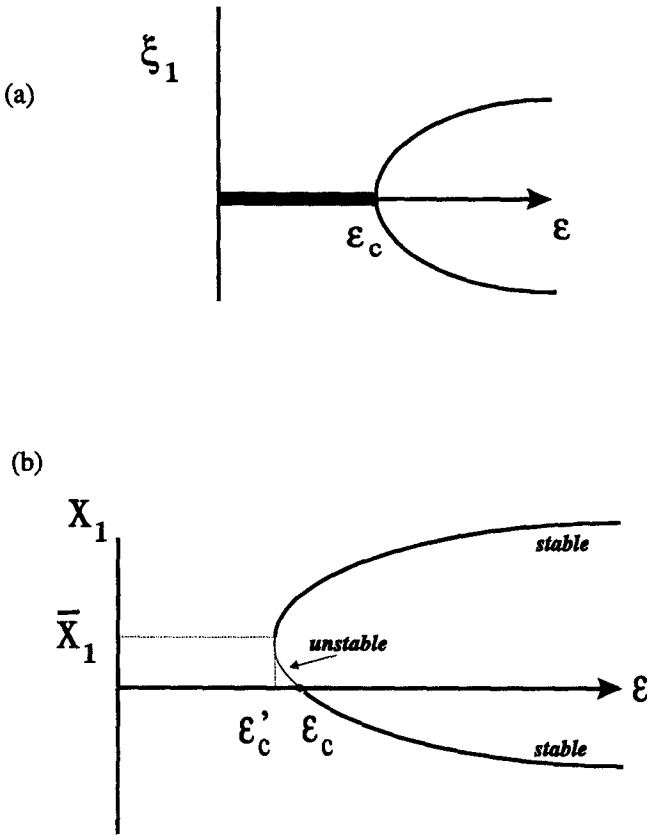

Fig. 8. **a** Supercritical bifurcations found in the analysis of the 2D case, and 3D cases. **b** Transcritical bifurcation predicted by equation (9.5) in the 3D double-humped kernel case

These results are in full agreement with the general scheme for symmetry break in systems with O(2) symmetry (see Friedrich and Haken, 1989; Busse 1987). Biologically, the results of the bifurcation analysis gives us the following pictures in the two dimensional case: In the case of the single-humped kernel, the steady state bifurcates into a distribution similar to $\cos(\theta)$, whereas in the double-humped case, it leads to a distribution similar to $\cos 2\ (\theta)$. This behaviour is illustrated in Fig. 9a,b.

9. Bifurcation analysis of Model I in 3D

The qualitative picture of the development of patterns in the 3D case following bifurcation is similar to the 2D case with one important exception. In the 3D case, the rotational symmetry group is O(3) which leads to rotational and pattern degeneracy, i.e. several eigenfunctions correspond to the same

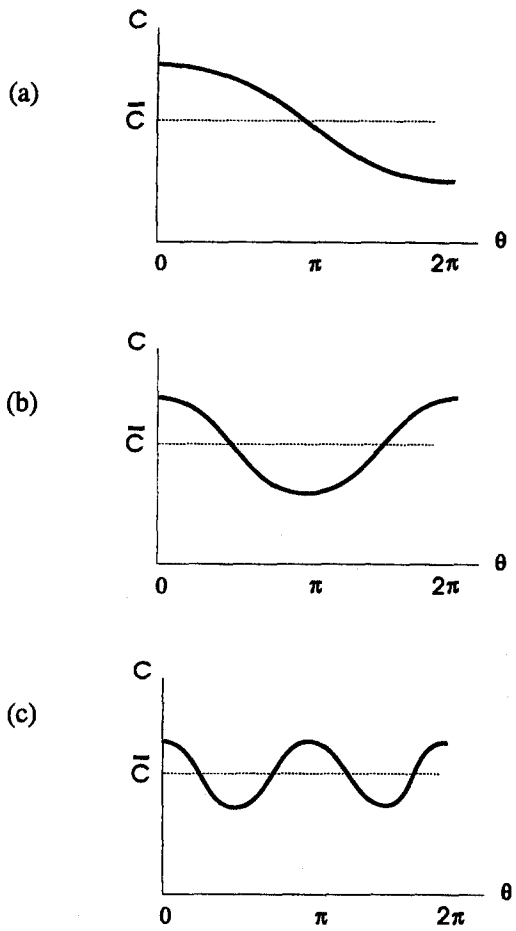

Fig. 9a–c. Types of patterns seen in the cell distribution in the 2D case after bifurcation. **a** A distribution similar to $\cos\theta$ which occurs in the case of a single-humped kernel. **b** A distribution similar to $\cos 2\theta$ occurs when the kernel is double-humped. **c** A distribution similar to $\cos 4\theta$ occurs in the case of orthogonal alignment kernels

eigenvalue. If the kernel is single-humped, then the first harmonic Y_1 responsible for the stability break is doubly rotationally degenerate. There is no pattern degeneracy in this case. These statements are true if we ignore the two-fold degeneracy over the associated Legendre polynomials, P_1^1, P_1^{-1} which differ in dependency over the angle θ, i.e.,

$$Y_1^1 = P_1^1(\cos\phi)\begin{cases}\cos\theta \\ \sin\theta\end{cases}, \tag{9.1}$$

where $Y_n^m = P_n^m(\cos\phi)\cos(m\theta)$. These can be neglected since different linear superpositions of $P_1^{\pm 1}$ just represent rotation about the axis of symmetry, thus

leaving the essential character of the solution unchanged. Furthermore, this degeneracy does not represent two different patterns. From group theoretic methods (Busse, 1987) it is known that the two harmonics Y_1^0 and Y_1^1 represent essentially the same state, just viewed from two different directions.

As before (in Sect. 8) we consider an expansion of C in terms of eigenfunctions, but now these are the Legendre polynomials, rather than simple trigonometric functions (see Appendix VI equation A6.1). We are now concerned with the amplitudes of two unstable harmonics, namely $P_1^0(\cos\phi)$, $P_1^1(\cos\phi)\cos(\theta)$ and we call these amplitudes z_1, z_2 respectively. We further use the notation $y_n(t), n = 2, \ldots$ to denote amplitudes of the stable harmonics. In the steady state, z_1, z_2, y_n are constants. We expect that the amplitudes of the stable modes again depend on the leading amplitudes, i.e. $y_n(t) = y_n(z_1(t), z_2(t))$. Close to criticality (when the governing parameter approaches its critical value) the stable mode amplitudes will be strongly dominated by the leading mode, so that we have one of the inequalities, $|y_n| \ll |z_1|$ or $|y_n| \ll |z_2|$ or both: $|y_n| \ll |z_i|$ $i = 1, 2, \ldots$

To find out what actually takes place in a given situation, we must find the first terms in the expansion for $y_n(z_i)$ and substitute them into the analogue of equation (8.6). (The form of this equation is the same but the leading partial derivative is replaced by the surface spherical Laplacian, (given by equation (A2.1).))

This will lead to a pair of ordinary differential equations for the amplitudes z_1, z_2 from which we can find the stable stationary solutions.

As in the 2D case, we keep terms up to third order, and arrive at an equation analogous to (A5.7). Thus, the method is in all respects analogous to the one described in Sect. 8. Because of the greater complexity in the 3D case, the analysis is formidable, and we do not here include details. Fortunately, we can use the results of [Busse, 1987 and references therein] where the general system with O(3) symmetry with quadratic nonlinearities was considered. Our equations are a particular case of this general system. We describe these general results below.

Let us chose $\phi = 0$ as the direction of the axis of symmetry of the pattern evolved. This means that the leading mode $P_1^0(\cos\phi) = \cos\phi$ takes over. In this case, in the stable stationary state $z_2 = 0$ and we have the estimate $z_0, y_2 \approx z_1^2$. The relative sizes of stable modes are given by $|y_n| \ll |y_2|, |z_0|$ for all $n \geqq 3$. The amplitude of the leading mode z_1 obeys the equation

$$\lambda z_1 - d z_1^3 = 0 \,, \tag{9.2}$$

where λ is the growth rate of unstable modes in the linear approximation, d is a coefficient of finite order depending on $\bar{C}, a, M, K_1, K_2$. Both λ and d are positive. We observe the similarity of this result to that of equation (8.14). The important fact is that the damping nonlinearity which stops the growth of the unstable mode, and causes its saturation is a cubic one.

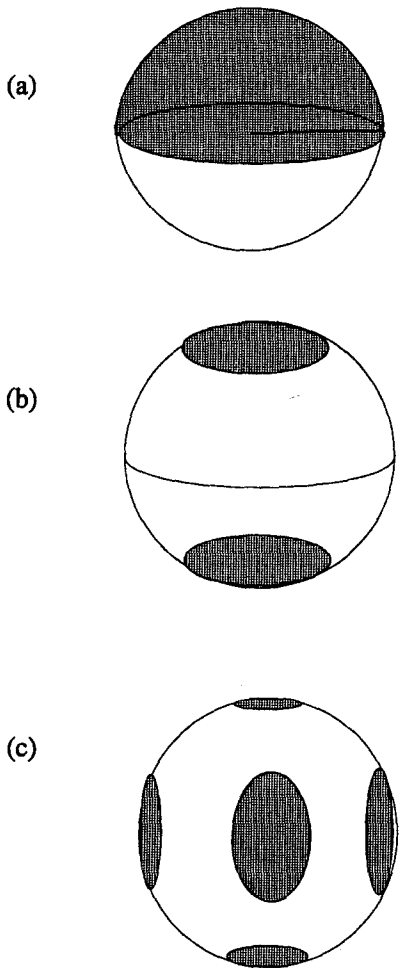

Fig. 10a–c. Three surface spherical harmonics that are significant in growing patterns in the 3D models. **a** P_1^0, **b** P_2^0, **c** Y_4^3: arises in the actin binding model where orthogonal interactions occur. The shaded regions on the sphere represent locations of increased density

The above equation has a stationary solution

$$z_1 = \pm\left(\frac{\lambda}{d}\right)^{1/2}. \tag{9.3}$$

The bifurcation is again supercritical, as shown in Fig. 10a.

From our choice of axis of symmetry, we have already noted that the leading mode $P_1^0(\cos\phi) = \cos\phi$ takes over. The pattern which starts to grow would therefore have the form shown in Fig. 10a. This type of pattern has the following property: the number of cells whose orientation is $\phi = \pi/2$ (i.e. the angular distribution at the equator of the spherical state-space) is unchanged, the number of cells at angles $\phi < \pi/2$ is increased, and most greatly at the pole $\phi = 0$. Conversely, the density of cells at $\phi > \pi/2$ diminishes, and particularly so at the pole $\phi = \pi$.

The case of the double humped kernel, is given in Appendix VI. There is a difference in that the leading mode possesses both orientational and pattern degeneracy. We consider the amplitudes x_1, x_2, x_3 of the modes containing terms of the form P_2^0, P_2^1, P_2^2 in the mode expansion of $C(\phi, \theta, t)$ (see Appendix VI equation A6.1). It can be shown that as a result of intermode interaction, the pattern degeneracy is removed: all non-axisymmetric harmonics die out.

Suppose we chose again $\phi = 0$ as the direction of the axis of symmetry of the pattern evolved. Then in the stable stationary state, the amplitudes $x_2 = x_3 = 0$ and $|x_0| \approx x_1^2$. We can arrive at the following equation for the leading mode amplitude:

$$\lambda x_1 + p_1 x_1^2 - p_2 x_1^3 = 0 , \tag{9.4}$$

where p_1 and $p_2 \simeq p_1$ are positive constants given in equation (A6.7) The stationary amplitude is then

$$x_1 = \begin{cases} \simeq -\lambda/p_1 \\ \simeq p_1/p_2 \end{cases} . \tag{9.5}$$

The important feature of this solution is that, as in the case of a single-humped kernel, pattern degeneracy disappears. The harmonics Y_2^1 and Y_2^2 die out and the only leading harmonic with amplitude significantly larger than all other harmonics is

$$P_2^0(\cos\phi) = \tfrac{1}{2}(3\cos^2\theta - 1). \tag{9.6}$$

The pattern evolved is axisymmetric. The expression (9.5) suggests that in this case, contrary to the 2D case (both single and double hump), and to the 3D single-humped case, we have a transcritical bifurcation as shown in Fig. 11. Examples in physical systems include liquid-solid or liquid-gas transitions.

In physical language, this means that we have a nonequilibrium phase transition of the first rather than second order. This leads to a number of important qualitative conclusions. One of these conclusions is that even before the bifurcation ($\varepsilon < \varepsilon_c$), there are values of the parameters ($\varepsilon_c' \leqq \varepsilon < \varepsilon_c$), such that the stable inhomogeneous pattern can co-exist with the stable homogeneous distribution. (Quantitative conclusions cannot be made from the diagram and formula (9.5) as the analysis is valid only at small amplitudes.)

This solution is characterized by the value $x_1 > 0$, so that the concentration of the cells around the equator decreases from the value $\phi \approx 55°$ to $\phi \approx 125°$, and the concentration of cells in the vicinity of the poles increases. See Fig. 10b. Then the amplitude of this pattern is not small, and it does not grow smoothly, as predicted in the 2D case in Sect. 8. Rather, the amplitude of the pattern jumps from zero to the values higher than $\bar{x}_1$ quite suddenly. The process is analogous to nucleation, which is well-known in physics. That is, a small perturbation can lead to massive recruitment and thus grows in size abruptly, as parameters leading to bifurcation change a little. (Our phenomenon, however, operates in angular rather than physical space.) If ($\varepsilon_c' < \varepsilon < \varepsilon_c$),

then, as a result of fluctuations which are larger as ε approaches ε_c, too many cells gather around the poles, leaving the equator, and the system relaxes to the nonhomogeneous pattern. After the bifurcation another stable pattern evolves at which the amplitude $x_1 \approx -\lambda/p_1$ is small and negative, so that the concentration of the cells decreases around the poles and increases around the equator.

The results of our nonlinear analysis are in qualitative agreement with the general mathematical results of pattern formation in systems with O(2) and O(3) symmetries [Friedrich and Haken, 1987; Busse, 1987] and well-known physical results on the character of phase transitions in ferro-electrics and liquid crystals [de Gennes, 1974; Chandrasekhar, 1977].

These results of nonlinear analysis apply to Models II and III.

Discussion

According to our linear stability analysis and bifurcation analysis, all three models in this paper lead to qualitatively similar results. This signifies some robustness in the modelling approaches. Not only are the results independent of the detailed assumptions about turning rate kernels, but also the types of forces or effects leading to turning do not significantly influence the behaviour.

We briefly comment on other applications of integro-partial differential equations in biological modelling. A review of integral equations in biology is given in Levin and Segel (1985).

One body of theory that has always relied heavily on the formulation and analysis of integral equations is the theory of activity and evolution of networks of biological neurons. An early example of this type of modelling is to be found in papers by Swindale (1980, 1982, 1991, etc) who describes development of patterns of ocular dominance or orientational response in cells of the visual cortex of mammals. Similarly, models that concern neural interactions and thus contain convolutions appear in Ermentrout and Cowan (1979), Ermentrout et al. (1986). In such models, the activation of a neuron at site x is in general dependent on inputs and stimuli arriving from neurons at remote sites, whose axons impinge on and synapse with the given local nerve cell. The type of effect of one neuron on another may typically depend on the mutual distance of the pair, and it is customary to assume that nearby neurons activate one another, whereas more distant ones have mutually inhibitory influences. For this reason, equations containing integral terms (which sum up the contributions of all neurons) with convolutions (that describe how the signal depends on the mutual distance) are convenient representations of these phenomena. Such equations do not come from balance arguments, and indeed the quantity of interest (which may be the intensity of activity) is not generally a conserved quantity. Many organisms do not move in a smooth continuous way, but rather execute a series of small bursts or discrete jumps that can have a variety of possible sizes. This type of motion has been modelled in the traditional equations of mass balance by inclusion of integral terms with

kernels that represent the jump size distribution. Examples of this approach include Alt (1988), Othmer et al (1988).

Integral equations have also appeared recently in the literature on coupled oscillators. An evolution equation for the density of oscillators at phase θ and frequency ω, analogous to a model by Kuramoto (1975) was derived and analyzed by Strogatz and Mirollo (1991). A review of the model is also presented in Strogatz (1993). Finally. an application of integral equaions to density of branches in a network of filaments that interact by cross-linking was investigated by Edelstein-Keshet and Ermentrout (1989).

We have remarked on the similarity of cell alignment to the alignment phenomena that is described in the physics literature: that of liquid crystals (see de Gennes, 1974). The particular case of nematic liquid crystals, in which the centers of mass of the molecules have no particular order, but in which there is some order in the directions of orientation of molecules is an apt analogy to the dense cultures of fibroblasts that exhibit patch alignment (Elsdale, 1972). Molecules in such structures can undergo random motion and tumbling, and they interact by electrostatic attraction or repulsion.

In cultures of fibroblasts, the random turning rates of the cells are analogous to the tumbling of molecules, resulting in a kind of angular diffusion. The cells however, are living units, with essentially "infinite resources of energy" on which to draw. Their interactions cannot be easily summarized with simple physics. The alignment of populations of cells is not an outcome of the shapes of the cells, but of the complex membrane and cellular cytoskeleton, and the dynamic response to contact with another cell.

Other papers in the physics literature which describe problems of pattern formation that are related to, but distinct from those we have outlined in this paper include Gross and Hohenberg (1993), Penrose (1978), San Miguel and Sagues (1990).

Appendix I. Linear stability, Model I

Equations (2.1) can be linearized about the homogenous steady state, $(\bar{C}, \bar{P})$ yielding

$$\begin{cases} \dfrac{\partial P}{\partial t}(\theta, t) = \beta_1 \bar{C} K * C + \beta_2 \bar{P} K * C + (\beta_1 \bar{C}) C - (\gamma - \beta_2 \bar{C}) P \ , \\ \dfrac{\partial C}{\partial t}(\theta, t) = \mu \dfrac{\partial^2 C}{\partial \theta^2} - \beta_1 \bar{C} K * C - \beta_2 \bar{C} K * P - (\beta_1 \bar{C} + \beta_2 \bar{P}) C + \gamma P \ . \end{cases} \tag{A1.0}$$

We investigate the stability of the homogeneous steady state by considering perturbations of the form

$$\begin{bmatrix} P(\theta, t) \\ C(\theta, t) \end{bmatrix} = \begin{bmatrix} \bar{P} \\ \bar{C} \end{bmatrix} + \begin{bmatrix} P_0 \\ C_0 \end{bmatrix} e^{in\theta} e^{\lambda t} \tag{A1.1}$$

Eigenfunctions

The set of eigenfunctions of the Laplacian in 1D, are

$$\psi_n(\theta) = e^{in\theta} \quad n = 0, 1 \ldots . \tag{A1.2}$$

That is, these functions have the property that

$$\Delta\psi_n = \frac{\partial^2 e^{in\theta}}{\partial\theta^2} = -n^2 e^{in\theta}. \tag{A1.3}$$

Thus the value $(-n^2)$ is the eigenvalue corresponding to the eigenfunction $\psi_n = e^{in\theta}$.

To show that these functions are also eigenfunctions of the linearized integral operator we note that by definition $\hat{K}$ is the Fourier transform of the function $K(\theta)$, so that

$$\hat{K}_n \equiv \int_{-\pi}^{\pi} K(\theta) e^{-in\theta} d\theta \,. \tag{A1.4}$$

This is equivalent to the identity

$$\int_{-\pi}^{\pi} K(-\theta') e^{in\theta'} \, d' = \hat{K}_n e^{in\theta} \,.$$

Thus inner product of the kernel with the eigenfunctions $e^{in\theta}$ of the Laplacian gives rise to a multiple of the same functions, i.e.

$$K * \psi_n = \hat{K}_n \psi_n, \quad n = 0, 1, \ldots \tag{A1.5}$$

establishing that they are also eigenfunctions of $K*$.

Single and double humped kernels

The results for the double-humped kernel can be obtained from the single-humped case by restricting the domain to $[-\frac{\pi}{2}, \frac{\pi}{2}]$. Then the distributions $P_s(\theta)$, $C_s(\theta)$ and $P_d(\theta)$, $C_d(\theta)$ (indexed by s for single-humped and d for double-humped kernel) are related by:

$$\begin{bmatrix} P_d(\frac{\theta}{2}) \\ C_d(\frac{\theta}{2}) \end{bmatrix} = \begin{bmatrix} P_s(\theta) \\ C_s(\theta) \end{bmatrix}, \quad \begin{bmatrix} P_d(\frac{\pi+\theta}{2}) \\ C_d(\frac{\pi+\theta}{2}) \end{bmatrix} = \begin{bmatrix} P_d(\frac{\theta}{2}) \\ C_d(\frac{\theta}{2}) \end{bmatrix}. \tag{A1.6}$$

Appendix II. Operators and eigenfunctions in 3D

The Laplacian operator in surface spherical coordinates has the form:

$$\Delta C(\theta, \phi, t) = \frac{1}{\sin\phi} \frac{\partial}{\partial\phi} \left(\sin\phi \frac{\partial C}{\partial\phi} \right) + \frac{1}{\sin^2\phi} \frac{\partial^2 C}{\partial\theta^2} \,. \tag{A2.1}$$

The convolutions expressed in terms of the angles ϕ and θ are

$$K * C \equiv \int_0^{\pi} \int_0^{2\pi} K(\phi, \theta, \phi', \theta') \, C(\phi', \theta') \sin\phi' d\theta' d\phi' \,. \tag{A2.2}$$

The Laplacian operator in surface spherical geometry has the eigenfunctions $Y_n(\phi, \theta)$ of degree n with

$$\Delta Y_n = -n(n+1)Y_n\,, \tag{A2.3}$$

Y_n can be expressed in the form:

$$Y_n(\phi, \theta) = A_0 P_n^0(\cos\phi) + \sum_{m=1}^{n} (A_m \cos m + B_m \sin m) P_n^m(\cos\phi)\,, \tag{A2.4}$$

where A_m's and B_m's are arbitrary constants, P_n^0 are Legendre polynomials of degree n, P_n^m are associated Legendre functions of degree n and order m. (Macrobert, 1967; Kraut, 1979.)

The first few Legendre polynomials for the case $m = 0$, P_n^0, (usually written simply P_n with the superscript omitted) written in terms of the argument $\cos\phi$ are:

$$\begin{cases} P_0(\cos\phi) \equiv 1, \\ P_1(\cos\phi) = \cos\phi\,, \\ P_2(\cos\phi) = \frac{3}{2}(\cos\phi)^2 - \frac{1}{2}\,. \end{cases} \tag{A2.5}$$

The inner products of the SSH with the Legendre polynomials are also SSH as follows:

$$\int_0^{2\pi}\int_{-1}^{1} P_n(\eta) Y_l(\phi', \theta') d(\cos\phi') d\theta' = \frac{4\pi}{2n+1} Y_n(\phi, \theta)\delta_{n,l}\,, \tag{A2.6}$$

where

$$\delta_{n,l} = \begin{cases} 1, & n = l\,; \\ 0, & n \neq l\,. \end{cases}$$

(See Macrobert (1967) or any classical text on spherical harmonics.) This means that

$$\int_S K(\Omega - \Omega') Y_n(\phi', \theta') d\Omega' = \hat{K}_n\, Y_n(\phi, \theta)\,, \tag{A2.7}$$

where

$$\hat{K}_n \equiv \hat{K}(n) = 2\pi \int_{-1}^{1} K(\eta) P_n^0(\eta) d\eta\,. \tag{A2.8}$$

This establishes that the SSH are eigenfunctions of both the Laplacian and the operator $K*$ in 3D.

Appendix III. Stability of the homogeneous steady state in 3D

In 3D, stability analysis of equations (4.4) to perturbations of the form (7.1) leads to a Jacobian matrix,

$$J = \begin{pmatrix} -\varepsilon & \xi \\ -\eta & -\delta \end{pmatrix}, \tag{A3.1}$$

where the constants stand for the following

$$\begin{aligned} \varepsilon &= \gamma - \beta\bar{C} \ , \\ \eta &= \gamma - \beta\bar{C}\hat{K}_n \ , \\ \xi &= \beta\bar{C}(1 + \hat{K}_n) + \beta\bar{P}\hat{K}_n \ , \\ \delta &= \mu n(n+1) + \beta\bar{C}(1 + \hat{K}_n) + \beta\bar{P} \ . \end{aligned} \tag{A3.2}$$

Thus, we find that in 3D

$$\det J = \beta\gamma \frac{\bar{C}^2}{\bar{P}} \left[\frac{\mu}{\gamma} n(n+1) - \left(\frac{\beta M}{\gamma} \right)^2 \hat{K}_n(1 - \hat{K}_n) \right], \tag{A3.3}$$

Thus, in 3D, instability occurs whenever

$$An(n+1) < \hat{K}_n(1 - \hat{K}_n), \qquad A = \frac{\mu}{\gamma} \left(\frac{\gamma}{\beta M} \right)^2 . \tag{A3.4}$$

Example kernels, Figs. 3 and 5

The exact functional forms of the kernels used to produce Figs. 3–5 were:

$$\begin{aligned} K_I &= \begin{cases} A_1(\cos\gamma - 3/4)^{-1/2} & \cos\gamma > 3/4 \ ; \\ 0, & \cos\gamma < 3/4 \ . \end{cases} \\ K_{II} &= \begin{cases} A_2, & \cos\gamma > 3/4 \ ; \\ 0, & \cos\gamma < 3/4 \ . \end{cases} \\ K_{III} &= \begin{cases} A_3 \cos[\frac{2\pi}{3}\gamma], & \cos\gamma > 3/4; \\ 0, & \cos\gamma < 3/4. \end{cases} \end{aligned} \tag{A3.5}$$

High harmonics are stable

Since A in equation (7.2) is positive, instability is most likely for low values of the integer n, e.g. $n = 1$ and high harmonics cannot destroy stability. This can be shown from the following estimate on the magnitudes of the RHS of the inequality for instability. We use the fact that

$$\| P_n(x) \| \leqq \sqrt{\frac{2}{\pi n}} (1 - x^2)^{-1/2} \tag{A3.6}$$

(see Abramowitz and Stegun, 1964; Macrobert 1967). Then it follows that

$$\hat{K}_n < \frac{C'}{\sqrt{n}}, \qquad \hat{K}_n(1 - \hat{K}_n) < \frac{C}{\sqrt{n}}, \tag{A3.7}$$

where C is some positive constant of order 1. So, if $n > n_c$, $n_c \approx A^{-1/2}$ then the nth harmonic would not destabilize the homogeneous distribution.

Kernel favoring instability and nonhomogeneous pattern

A particular form of the kernel, which would be most favorable to the existence of a non-homogeneous solution is:

$$\tilde{K}(\phi) = \begin{cases} \frac{1}{2\pi}\cos\phi + K_A(\phi), & \phi = \theta \quad \text{in 2D}, \\ \frac{3}{8\pi}\cos\phi + K_B(\phi), & \phi = \gamma \quad \text{in 3D}, \end{cases} \tag{A3.8}$$

where $K_{A,B}$ are orthogonal to $\cos\phi$ and their exact form is not important. (When $\hat{K}_1(1 - \hat{K}_1) = 1/4$ then symmetry breaks at $A > 1/4$ in 2D and $A > 1/8$ in 3D.)

Appendix IV. Results for the actin-binding kernel

In this appendix we will briefly describe the results on orthogonal alignment that occurs in the actin model. It is natural to assume, based on our experience with the single and double humped kernels, that an even, nonnegative double humped kernel having humps at $-\pi/2$ and $\pi/2$ leads to orthogonal alignment. (Alignment occurs along angles where the kernel has maxima.) An example of this type of kernel is shown in Fig. 1c. Because of the periodicity of the kernel (period is π), only the coefficients $\hat{K}_n$ with n even are nonzero in the Fourier expansion for the kernel in the 2D case, and expansion over spherical harmonics in the 3D case. It is important that both in 2D and in 3D, $\hat{K}_2 < 0$, $\hat{K}_2(1 - \hat{K}_2) < 0$ and $0 < \hat{K}_4 < 1$. This means that the second harmonic is stable and in general it will be the fourth harmonic that breaks stability and becomes the leading mode. (See also Civelekoglu and EK, 1993). This result holds for all three models considered in the present paper.

In the 2D case, the bifurcational analysis close to criticality is analogous to the one we have carried out in Sect. 6. The bifurcation is supercritical, and

$$C(\theta) \approx \bar{C} + k\sqrt{|\varepsilon - \varepsilon_c|}\cos(4\theta) .$$

See Fig. 9c.

In the 3D case, where again, the fourth harmonics Y_4 is unstable, the leading mode is highly degenerate, both rotationally and patternwise. The mode competition leads to the removal of the pattern degeneracy, however, so the axisymmetric solution loses its preferential status. (It dies out as a result of competition.) The pattern evolved has the form of six mutually perpendicular smooth bumps in the distribution of Actin fibers on the surface of the sphere (see Fig. 9c). The bifurcation as in the 3D, double humped case is of transcritical character.

Appendix V. Synergetic analysis of Model I in 2D

Under the assumptions given in Sect. 8, we can perform the calculations shown below. First, we form the expansion

$$\begin{pmatrix} C(\theta, t) \\ P(\theta, t) \end{pmatrix} = \begin{pmatrix} \xi_1(t) \\ \eta_1(t) \end{pmatrix} v_1(\theta) + \sum_{i=2}^{\infty} \begin{pmatrix} \xi_i(t) \\ \eta_i(t) \end{pmatrix} v_i(\theta) + \begin{pmatrix} \bar{C} \\ \bar{P} \end{pmatrix}. \tag{A5.1}$$

(Note that $v_i(\theta)$, $i = 2, \ldots$ are either $\cos(i)$ or $\sin(i)$ for integer i, and $(\xi_i(t), \eta_i(t))$ are their amplitudes as functions of time, assumed to depend on the amplitude of the first mode):

$$\begin{pmatrix} \xi_i(t) \\ \eta_i(t) \end{pmatrix} = \begin{pmatrix} \xi_i[\xi_1(t), \eta_1(t)] \\ \eta_i[\xi_1(t), \eta_1(t)] \end{pmatrix} \quad i = 2, 3, \ldots \tag{A5.2}$$

Close to criticality, the expression (A5.2) is valid.

We can form a valid asymptotic expansion for $(\xi_i(t), \eta_i(t))$ $i = 2, 3, \ldots$ in powers of (ξ_1, η_1):

$$\xi_i(t) = \sum_{J_1, J_2 = 0}^{\infty} c_{J_1, J_2} \xi_1(t)^{J_1} \eta_1(t)^{J_2}. \tag{A5.3}$$

A similar expression holds for $\eta_i(t)$.

We look for a solution of equations (8.6, 8.7) in the form

$$C(\theta) = \bar{C} + \xi(\theta), \qquad \xi(\theta) = \sum_{i=0}^{\infty} \xi_i v_i(\theta), \quad |\xi(\theta)| \ll \bar{C} \tag{A5.4}$$

derived from the expansion (A5.1) that is, in which the deviation away from the homogenous state is expressed as a superposition of the harmonics, as indicated above. If we restrict attention to the linear approximation, we get equation (8.9). Substituting in the Fourier series expansion for $\xi(\theta)$ given in equation (A5.4), using the fact that $K * v_n = \hat{K}_n v_n$ for every $n = 1, 2, \ldots$ and equating coefficients of each harmonic on both sides of the resulting equation, we obtain the following system of equations:

$$\left(-n^2 \varepsilon + \frac{a\bar{C}^2}{(a - \bar{C})^2} \hat{K}_n (1 - \hat{K}_n) \right) \xi_n = 0 \quad n = 1, 2, 3 \ldots \tag{A5.5}$$

The expression multiplying ξ_n in equation (A5.5) coincides with the one for the determinant of the stability matrix, so we can rewrite the above equation in the form:

$$\lambda_n \xi_n = 0, \quad n = 1, 2, \ldots \tag{A5.6}$$

These equations have only trivial solutions, which indicates that the linear approximation is not sufficiently informative. Keeping terms up to third order in ξ leads to the nonlinear equation. In this approximation equation (8.9) has

the form:

$$\varepsilon\Delta\xi + \frac{a\bar{C}^2}{f^2}[(K*\xi - K*(K*\xi)] + \left[\frac{a^2\bar{C}}{f^3}(K*\xi)^2 - \frac{a\bar{C}}{f^2}\xi(K*(K*\xi)) + \frac{a\bar{C}}{f^2}\xi(K*\xi) - \frac{a\bar{C}^2}{f^3}K*((K*\xi)^2) - \frac{a\bar{C}}{f^2}K*(\xi(K*\xi))\right]$$

$$+ \left[\frac{a^2\bar{C}}{f^4}(K*\xi)^3 - \frac{a\bar{C}^2}{f^4}K*((K*\xi)^3) - \frac{a\bar{C}}{f^3}K*(\xi(K*\xi)^2) + \frac{a^2}{f^3}\xi(K*\xi)^2 - \frac{a\bar{C}}{f^3}\xi K*((K*\xi)^2) - \frac{a}{f^2}\xi K*(\xi(K*\xi))\right] = 0\,, \tag{A5.7}$$

where $f \equiv a - \bar{C}$. We substitute the expansion (A5.4) into (A5.7) and keep terms up to third power in ξ_1 and up to second power in ξ_i, $i = 1, 2, \ldots$ We use trigonometric identities to simplify expressions involving products of the harmonics, (i.e. identities for products of sines and cosines) and equate coefficients of each harmonics on both sides of the equation as before. We get the hierarchical system of equations (8.11).

The expressions for constants appearing in equations (8.11) and (8.12) are as follows:

$$\begin{cases} A_1 = \dfrac{a\bar{C}}{2f^2}\hat{K}_1(1-\hat{K}_1) \\ |\lambda_2| = \dfrac{a\bar{C}^2}{(a-\bar{C})^2}(4\hat{K}_1(1-\hat{K}_1) - \hat{K}_2(1-\hat{K}_2)) \\ B_2 = \dfrac{a\bar{C}}{f^2}\hat{K}_1(1-\hat{K}_1)\left(1 - \dfrac{\bar{C}}{f}\hat{K}_1\right) \\ G = \dfrac{2a^2\bar{C}}{f^3}\hat{K}_1(1-\hat{K}_1) \\ B_1 = \dfrac{a\bar{C}}{f^2}\left[\dfrac{a+\bar{C}}{a-\bar{C}}\hat{K}_1\hat{K}_2 - 2\hat{K}_1^2 - \hat{K}_2^2 + \hat{K}_1 + \hat{K}_2 - \dfrac{2\bar{C}}{f}\hat{K}_1^2\hat{K}_2\right] \\ F = \dfrac{a\bar{C}\hat{K}_1^2}{f^3}\hat{K}_1^2(1-\hat{K}_1)\left(1 + \dfrac{\bar{C}}{f}\hat{K}_1\right) \\ D = GA_1 - F + \dfrac{B_1B_2}{|\lambda_2|} \end{cases} \tag{A5.8}$$

where

$$\bar{C} = \frac{aM}{a+M} . \tag{A5.9}$$

Double humped kernel

In the case of a double humped kernel we have an expansion over the even harmonics only. The expansion has the form:

$$C(\theta) = \bar{C} + \xi_2^1 v_2(\theta) + \sum_{n=2}^{\infty} \xi_{2n}^1 v_{2n}(\theta) , \tag{A5.10}$$

$$\xi_2^1 = \pm k' \sqrt{|\varepsilon - \varepsilon_c'|}, \qquad |\xi_{2n}^1| = k_{2n}' |\varepsilon - \varepsilon_c'|^{n/2}, \quad n = 2, 3, \ldots \tag{A5.11}$$

where k', k_{2n}', ε_c' have the same meanings as before. The character of the bifurcations is the same.

Appendix VI. Bifurcation analysis of Model I in 3D

We consider an expansion of C in terms of the eigenfunctions (Legendre polynomials).

$$C(\phi, \theta, t) = \bar{C} + z_0 + z_1(t)\, P_1^0(\cos\phi) + z_2(t)\, P_1^1(\cos\phi)\cos(\theta) + \sum_{n=2}^{\infty} y_n(t)\, Y_n(\phi, \theta) , \tag{A6.1}$$

where we define the norm

$$|Y_n| = \max_m |Y_n^m| , \tag{A6.2}$$

and where z_1, z_2 are amplitudes of the two unstable harmonics, and $y_n(t)$, $n = 2, \ldots$ are amplitudes of the stable harmonics.

Double humped kernel In the case of the double humped kernel, the leading mode possesses both orientational and pattern degeneracy.

$$Y_2 = x_1 P_2^0 + x_2 P_2^1 + x_3 P_2^2 , \tag{A6.3}$$

we have the decomposition

$$C(\phi, \theta, t) = \bar{C} + x_0(t) + x_1(t) P_2^0(\phi) + x_2(t) P_2^1(\phi)\cos\theta + x_3(t) P_2^2(\phi)\cos 2\theta + \sum_{2n, n=2}^{\infty} \rho_{2n}(t)\, Y_{2n}(\phi, \theta) , \tag{A6.4}$$

$$\rho_n Y_n = \{\rho_n^m Y_n^m\} \quad m = 0, \ldots, n, |\rho| = \max_m |\rho_n^m| . \tag{A6.5}$$

As a result of intermode interaction, the pattern degeneracy is removed: all non-axisymmetric harmonics die out and if we chose again $\phi = 0$ as the direction of the axis of symmetry of the pattern evolved, then in the stable

stationary state, $x_2 = x_3 = 0$, $|\rho_4|, |x_0| \approx x_1^2$, $|\rho_n| \ll x_1^2$, $n \geqq 4$, and the leading mode amplitude obeys the equation

$$\lambda x_1 + p_1 x_1^2 - p_2 x_1^3 = 0 \,, \tag{A6.6}$$

where

$$p_1 = \frac{4}{49} \frac{a^2 \bar{C}}{(a - \bar{C})^3} \hat{K}_2^2 (1 - \hat{K}_2) > 0, \quad p_2 \sim p_1 > 0 \tag{A6.7}$$

Acknowledgements. LEK is funded by a Natural Sciences and Engineering Research Council (Canada) Operating grant. AM is holding a University Graduate Fellowship scholarship from the University of British Columbia. This research and scientific exchange with Dr W. Alt (Bonn, Germany) is being supported by a NATO collaborative research grant to LEK.

References

1. Alt W (1988) Modelling of motility in biological systems, ICIAM 1987 Proceedings, SIAM Philadelphia, pp 15–30
2. Alt, W and Giegant E (1994) private communication
3. Abramowitz M, Stegun A, eds (1964) Handbook of Mathematical Functions, Nat Bureau of Standards, Washington
4. Busse F H (1987) Patterns of bifurcation from spherically symmetric cases, in: Guttinger W, Dangelmayr G, eds, The Physics of Structure Formations, Springer, NY, pp. 88–96
5. Civelekoglu, G, Edelstein-Keshet L (1994) Models for the formation of Actin Structures, in press
6. Chandrasekhar S, Shashihad R, Tara N (1970) Theory of melting of molecular crystals: the liquid crystalline phase, Molec Cryst Liq Cryst **10**: 337–358
7. de Gennes P G (1974) The Physics of Liquid Crystals, Claredon Press, Oxford
8. Edelstein-Keshet L, Ermentrout G B (1989) Models for branching networks in two dimensions, SIAM J Appl Math **49** (4): 1136–1157
9. Edelstein-Keshet L, Ermentrout G B (1990) Models for contact-mediated pattern formation: cells that form parallel arrays, J Math Biol **29**: 33–58
10. Elsdale T (1972) Pattern formation in fibroblast cultures, an inherently precise morphogenetic process, in: Towards a Theoretical Biology 4, C H Waddington (ed), Edinburgh University Press
11. Elsdale T and Wasoff F (1976) Fibroblast cultures and dermatoglyphics: the topology of two planar patterns, Wilhelm Roux's Archives **180**, 121–147
12. Ermentrout B, Campbell J, Oster G (1986) A model for shell patterns based on neural activity, The Veliger **28** (4): 369–388
13. Ermentrout G B, Cowan J (1979) A mathematical theory of visual hallucination patterns, Biol Cyber **34**, 137–150.
14. Friedrich R, Haken H (1989) A short course on synergetics, in: A N Proto, ed, Nonlinear Phenomena in Complex Systems, Elsevier, North Holand, pp 103–150
15. Greco F, Marrucci G (1992) Rodlike molecular dynamics, the tumbling regime, Mol Crystals Liq Crystals **212**: 125–137
16. Gross, M C Hohenberg P C (1993) Pattern formation outside of equilibrium, Rev Mod Phys **65** (3): 851–112
17. Grunbaum D (1994) Swarming behaviour as an aide to Chemotaxis, in: Parrish J, Hammner W, 3D Animal Aggregations, Cambridge University Press
18. Haken H (1977) Synergetics, Springer NY
19. Hunding A (1982) Spontaneous biological pattern formation in 3D sphere. Prepatterns in mitosis and cytokinesis, in: H Haken, ed, Evolution of Order and Chaos, Springer, Berlin, p 100

20. Katz L C, Potel M J, Wasserung R J (1981) Structure and mechanism of schooling in tadpoles of the clawed frog, Xenopus laevis, Anim Behav **29**: 20–33
21. Kraut E A (1979) Fundamentals of Mathematical Physics, Kreiger Publ, NY
22. Kuramoto Y (1975) Self-entrainment of a population of coupled nonlinear oscillators. In: International Symposium on Mathematical Problems in Theoretical Physics. H Araki, ed (Lecture Notes in Physics, vol **39**) Springer, NY, 420–422
23. Levin S A, Segel L A (1985) Pattern generation in space and aspect. SIAM Review **27**, 45–67
24. Luckhurst G R, Gray G W (1979) The Molecular Physics of Liquid Crystals, Acad Press, NY
25. Macrobert T M (1967) Spherical Harmonics, Pergamon Press, Oxford
26. Mogilner A, Edelstein-Keshet L (1994) Spatio-angular order in populations of self-aligning objects: formation of oriented patches. Submitted for publication
27. Murray J D (1989) Mathematical Biology, Springer Verlag, NY
28. O'Brien D P (1989) Analysis of the internal arrangement of individuals within crustacean aggregations (Euphausiacea, Mysidacea), J Exp Mar Biol Ecol **128**: 1–30
29. Onsager L (1949) The effects of shape on the interaction of colloidal particles, Ann NY Acad Sci **51**: 627–659
30. Othmer H G, Dunbar S R, Alt W (1988) Models of dispersal in biological systems, J math Biol **26**: 263–298
31. Penrose O (1978) Kinetics of phase transitions, in: Garrido L, et al. eds, Stochastic Processes in Nonlinear Systems, Springer, NY, p 211
32. Priestly E B, Wojtowicz P J, Cheng P, eds (1975) Introduction to Liquid Crystals, Plenum Press, NY
33. San Miguel M, Sagues F (1990) Transient pattern Dynamics, in: Walgraef D, Ghoniem N M, eds, NATO Advanced Study Institute on Patterns, Defects, and Material Instabilities (Cargese, France, 1989) Kluwer Publ, Dordrecht, Netherlands
34. Sheng P (1973) Effects of bundling in a lattice gas model of liquid crystals, J Chem Phys **59**: 1942–1952
35. Strogatz S H (1993) Norbert Wiener's brain waves. in Lecture Notes in Biomathematics 100, Springer Verlag
36. Strogatz S H, Mirollo R E (1991) Stability of incoherence in a population of coupled oscillators. J Stat Phys **63**: 613–635
37. Swindale N V (1980) A model for the formation of ocular dominance stripes, Proc. R. Soc London B **208**: 243–264
38. Swindale N V (1982) A model for the formation of orientation columns, Proc R Soc London B **215**: 211–230
39. Swindale N V (1991) Coverage and the design of striate cortex, Biol Cybern **65**: 415–424
40. Swindale N V (1992) A model for the coordinated development of columnar systems in primate striate cortex, Biol Cybern **66**: 217–230